NTIA Report 15-515

Effect of Broadband Radio Service Reallocation on 2900–3100 MHz Band Marine Radars: Front-end Overload

Robert Achatz
Mark McFarland
Roger Dalke
Geoffrey Sanders
Paul McKenna,
Frank Sanders
Robert Johnk

report series

U.S. DEPARTMENT OF COMMERCE • National Telecommunications and Information Administration

NTIA Report 15-515

Effect of Broadband Radio Service Reallocation on 2900–3100 MHz Band Marine Radars: Front-end Overload

Robert Achatz
Mark McFarland
Roger Dalke
Geoffrey Sanders
Paul McKenna,
Frank Sanders
Robert Johnk

U.S. DEPARTMENT OF COMMERCE

April 2015

DISCLAIMER

Certain commercial equipment and materials are identified in this report to specify adequately the technical aspects of the reported results. In no case does such identification imply recommendation or endorsement by the National Telecommunications and Information Administration, nor does it imply that the material or equipment identified is the best available for this purpose.

CONTENTS

FIGURES

TABLES

ACRONYMS

3GPP 3rd Generation Partnership Project

ALC Automatic level control

APD Amplitude probability distribution

AWGN Additive white Gaussian noise

BPF Bandpass filter

BRS Broadband radio service

BW Bandwidth

CFAR Constant false alarm rate

CW Continuous wave

dB Decibel

dBi Decibels relative to the gain of an isotropic antenna

dBm Decibels relative to a milliwatt

dBsm Decibels relative to a square meter

dBW Decibels relative to a watt

DOD Department of Defense

DP Degradation point

DUT Device under test

EIRP Effective isotropic radiated power

ETSI European Telecommunications Standards Institute

FDD Frequency division duplex

FDR Frequency dependent rejection

FE Front-end

FEF Front-end filter

FS Free space

GCP Gain compression point

GHz Gigahertz

GN	Gaussian noise
Hz	Hertz
IEC	International Electrotechnical Committee
IEEE	Institute of Electrical and Electronics Engineers
IF	Intermediate frequency
INR	Interference to noise power ratio
IPC	Interference protection criteria
ITM	Irregular terrain model
ITS	Institute for Telecommunication Sciences
ITU	International Telecommunication Union
ITU-R	ITU Radiocommunication Sector
kHz	kilohertz
km	Kilometer
LNA	Low-noise amplifier
LNFE	Low-noise front-end
LTE	Long Term Evolution
MHz	Megahertz
MIMO	Multiple-input multiple-output
MSC	Maritime Safety Committee
NEP	Noise enhancement point
nmi	Nautical mile
ns	Nanosecond
NTIA	National Telecommunications and Information Administration
NVWFM	Non-volatile waveform memory
OFDM	Orthogonal frequency division multiplexing
OFDMA	Orthogonal frequency division multiple access
OOB	Out-of-band

PM Power meter

PRF Pulse repetition frequency

PRI Pulse repetition interval

PSD Power spectral density

RCS Radar cross section

RF Radio frequency

RPM Revolutions per minute

SA Spectrum analyzer

SA Spectrum analyzer

SG Signal generator

SINR Signal to interference plus noise ratio

SMA Sub-miniature version A (connector)

SNR Signal to noise ratio

SOLAS Safety of life at sea

STC Sensitivity time control

TDD Time division duplex

UMTS Universal Mobile Telecommunications System

UN United Nations

UN/MSC United Nations Maritime Safety Committee

USCG United States Coast Guard

VSA Vector signal analyzer

VSA Vector signal analyzer

VSG Vector signal generator

WGN White Gaussian noise

WiMAX Worldwide interoperability for microwave access

EXECUTIVE SUMMARY

Spectrum reallocation is often necessary to accommodate new services which can potentially increase business productivity and enhance the lives of private citizens. However, reallocating services to bands near those used by incumbent services—or, in some cases, to those same bands—can cause interference to the incumbent service.

Spectrum reallocation can cause interference in radar systems in a number of ways. A system reallocated to a nearby band can introduce unwanted signals into the radar detection bandwidth. Also, a system reallocated to a nearby band can overload the radar receiver front-end and cause gain compression, increased noise power, and intermodulation in the radar detection bandwidth.

The U.S. Coast Guard (USCG) asked the National Telecommunications and Information Administration Institute for Telecommunication Sciences (NTIA/ITS) to investigate effects of reallocation on the 2900–3100 MHz band marine radar service by determining interference protection criteria (IPC) and analyzing strategies for mitigating the interference.

Here we investigate the effects of reallocation to accommodate broadband radio services (BRS) on the 2900–3100 MHz band marine radar service. The BRS is the next generation of personal communications services which will provide wideband Internet communications to mobile users. Results of our investigations have been assembled into three reports subtitled “Background,” “Unwanted Emissions,” and “Front-end Overload.”

This report describes a methodology for analyzing magnetron radar receiver front-end overload caused by signals from an aggregate of broadband radio service (BRS) base stations transmitting at frequencies within the radar front-end bandwidth.

The analysis in this report determines how much front-end filter attenuation is needed for various separation distances. The attenuation is the difference between the interfering power at the radar low-noise front-end (LNFE) and the allowable interference power.

The interfering power present at the LNFE is determined with a propagation model and a methodology for aggregating the signals from a network of base stations. Because of non-linear analytic complexity, allowable interference power, I_a, is determined by probability of detection laboratory measurements.

Two front-ends were examined. The first was an off-the-shelf magnetron radar front-end assembly with a circulator, limiter, and low-noise front-end. The second was what we refer to as a reference front-end consisting of a low-noise front-end constructed from discrete RF components. The reference front-end had approximately the same characteristics as the magnetron front-end assembly. However, the reference front-end did not have the filtering provided by the magnetron front-end assembly circulator and limiter.

The 5% degradation point (5% DP) measurements found I_a to be -11.5 and -9 dBm for the reference front-end and magnetron front-end assembly, respectively. Propagation analysis showed that interference powers were less than -23.6 dBm at a 1 km separation distance from the closest base station. Consequently, the front-end does not need filter attenuation for distances as

close as 400 meters. Distances less than 400 meters were not analyzed due to antenna near field effects. Since the magnetron front-end assembly I_a is greater than the reference front-end's, this result would be true for the magnetron front-end assembly as well.

Gain compression and noise enhancement metrics, which are simpler to measure than the 5% DP metric, were also evaluated to determine if they could reliably predict I_a. We found that only the noise enhancement metric predicted it for both front-ends. This result is important since many front-end overload studies are based on the gain compression metrics.

The results in this report are encumbered with two caveats. First, the results are for an FDD BRS base station signal that occupies one 10 MHz BRS channel. Results need to be adjusted to accommodate more channels. Second, these results are based on magnetron radar signal processing. Additional analysis is needed to assess the impact to solid state radar receivers because their signal processing is very different from that in the magnetron radar receivers. The signal processing affects sensitivity and estimates of front-end attenuation need to take this into account.

EFFECTS OF BROADBAND RADIO SERVICE REALLOCATION ON 2900–3100 MHZ BAND MARINE RADARS: FRONT-END OVERLOAD

Robert Achatz, Mark McFarland, Roger Dalke, Geoffrey Sanders, Paul McKenna, Frank Sanders, Robert Johnk[1]

Spectrum reallocations may place broadband radio services (BRS) near spectrum used by 2900–3100 MHz band marine radars. Signals from the BRS base stations can potentially cause the radar front-end to overload and cause interference. This report provides a method that can be used to estimate front-end filter attenuation required at various radar to base station separation distances. The attenuation is the difference between the interfering power at the radar low-noise front-end (LNFE) and the allowable interference power. The BRS signal was emulated with 10 MHz bandwidth Gaussian noise. The allowable interference power IPC is determined from probability of detection measurements with a custom test fixture. Two front-ends were tested. One was an off-the shelf magnetron radar front-end assembly consisting of a circulator, limiter, and low-noise front-end. The other, referred to as the reference front-end, was constructed of discrete components. The reference front-end was tested without the frequency selectivity of the circulator and limiter. Results showed that the allowable interference power is -11.5 and -9 dBm for the reference front-end and magnetron front-end assembly, respectively. Additional front-end filtering is not required for either front-end at distances as close as 400 meters. Distances less than 400 meters were not analyzed due to near-field effects. Gain compression and noise enhancement metrics, which are simpler to measure than performance degradation, were also evaluated to determine if they could reliably predict allowable interference power. Only the noise enhancement metric could reliably predict the performance degradation. This result is important since many front-end overload studies are based on the gain compression point metrics.

Keywords: broadband radio service, front-end filter, front-end overload, gain compression, interference, interference protection criteria, marine radar, noise enhancement, radar, radio spectrum engineering, radio wave propagation

1 INTRODUCTION

Spectrum reallocation is often necessary to accommodate new services which can potentially increase business productivity and enhance the lives of private citizens. However, reallocating services to bands near those used by incumbent services—or, in some cases, to those same bands—can cause interference to the incumbent service.

Spectrum reallocation can cause interference in radar systems in a number of ways [1], [2], [3], [4]. For example, a system moved to a nearby band can introduce unwanted emissions into the radar detection bandwidth. Also, emissions from a system reallocated to a nearby band can overload the radar receiver front-end (receiver circuits operating at the carrier frequency) and

[1] The authors are with the Institute for Telecommunication Sciences, National Telecommunications and Information Administration, U.S. Department of Commerce, Boulder, CO 80305.

cause gain compression, increased noise power, and intermodulation in the radar detection bandwidth.

The U.S. Coast Guard (USCG) asked the National Telecommunications and Information Administration Institute for Telecommunication Sciences (NTIA/ITS) to investigate effects of spectrum reallocation on the 2900–3100 MHz band marine radar service by determining interference protection criteria (IPC) and analyzing strategies for mitigating the interference.

Results of these investigations are expected to be useful to regulatory and standards bodies which are responsible for developing IPC including the NTIA [5]; the International Telecommunication Union (ITU) [6]; the International Electrotechnical Commission (IEC) [7], which is currently devising IPC tests on behalf of the United Nations Maritime Safety Committee (UN/MSC) [8]; and the Institute of Electrical and Electronics Engineers (IEEE) [9].

In this series of reports we analyze the effects of reallocation to accommodate broadband radio services (BRS) on the 2900–3100 MHz band marine radar service. The BRS is the next generation of personal communications services which will provide wideband Internet communications to mobile users. Spectrum regulators are currently investigating various reallocation strategies to accommodate BRS growth.

Marine radars are used by ships to avoid collisions with objects while traveling in oceans, seas, lakes, and rivers. An example of a marine radar antenna mounted on a ship is shown in Figure 1. Detection of objects, referred to as targets, is often difficult. Even on calm seas, the target can have significant radar cross section (RCS) variation and corresponding reductions in signal power. The target can also be obscured by signal reflections or clutter from waves and precipitation.

These 2900–3100 MHz band radars are often referred to as S-band marine radars. Similar radars that operate in the 9200–9500 MHz band are often referred to as X-band marine radars. The primary advantage of S-band radar signals is that they have less precipitation attenuation than X-band radar signals. This allows S-band radars to detect smaller objects at longer distances in adverse weather conditions. Large ships subject to international safety of life at sea (SOLAS) regulations generally operate with radars in both bands.

BRS providers promise to deliver fast, reliable Internet service to users wherever they are. An example of a BRS base station is shown in Figure 2. Potential unwanted emissions and front-end overload problems in 2900–3100 MHz band marine radars from BRS base stations were brought to the attention of the International Telecommunication Union in November 2009 by the United Kingdom [10].

Significant amounts of spectrum are needed for widespread BRS use. BRS systems are already operating in the 2500–2690 MHz band. The 3500–3650 MHz band has been evaluated for reallocation [11]. Other reallocations in the 2700–3700 band, currently allocated to a number of radar services as shown in Figure 3, could also affect 2900–3100 MHz band marine radars.

BRS and radar system characteristics are derived from those used by internationally recognized groups. The BRS system is modeled after systems devised by the European Technical Standards Institute (ETSI) Universal Mobile Telecommunications System (UMTS) committee/3rd

Generation Partnership Project (3GPP) [12], ITU [13], and the WiMAX Forum [14]. The radar system is modeled after a system devised by the IEC 62388 standard shipborne radar committee [7] for industry acceptance testing.

Figure 1. Marine radar slotted array antenna (white bar) mounted on motor which spins it.

Figure 2. BRS base station.

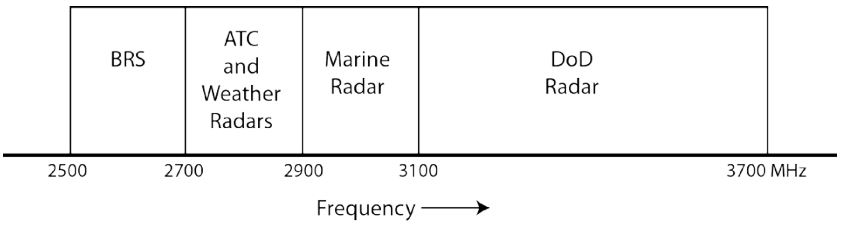

Figure 3. Radio spectrum from 2500 to 3700 MHz with current allocations for air traffic control (ATC), weather, marine, and various Department of Defense (DOD) radar services.

1.1 Previous Background Work

The IPC, scenario, and models needed for interference analysis are provided in the previous background report [15] and briefly summarized here. IPC are needed to reduce the probability of collision while not placing onerous burdens on other systems using the radio spectrum. Our objective is to determine IPC and factors such as distance and frequency separation that can mitigate the effects of the interfering signal so IPC can be met. IPC for base station interference in the marine radar receiver include:

Radar baseline performance level, signal to noise ratio (SNR), and reliability

Radar allowable degraded performance level, interference power level, and reliability

The physical scenario used for interference analysis is shown in Figure 4. We assume a radar target is located between a network of BRS base stations and a ship with a 2900–3100 MHz band magnetron marine radar. Weather conditions are assumed to be benign so that there is no signal "clutter" from reflections off precipitation or waves.

Radar targets include shorelines, ships, boats, and navigational buoys. The target RCS, which varies or fluctuates with time, is modeled with a statistical distribution. The mean of the distribution is dependent on target aspect angle, shape, and materials.

The base stations are modeled after those described by ETSI UMTS, 3GPP, ITU, and WiMAX groups. BRS signals use orthogonal frequency division multiple access (OFDMA) and are transmitted within BRS channels characterized by their center frequency and bandwidth. Transmit and receive signals use frequency division duplexing (FDD) so that transmissions can occur at all times. The signals are transmitted from antennas that typically cover 60 degree azimuth sectors with slant, 45 degree polarization. Although more than one BRS channel can be transmitted at one time, we assume only one 10 MHz channel is transmitted.

The radar is modeled after the magnetron radar in the IEC 62388 standard for shipborne radars. The radar transmits periodic pulses from a rotating antenna with a narrow antenna beam width and horizontal polarization. Typically short, medium, and long pulse widths are used to detect targets at different ranges and range resolution. Pulses arriving within the time it takes the antenna to traverse its beam width are integrated to enhance SNR.

The interfering radio wave propagation path is the path from the base station to the radar. The desired propagation path is the path from the radar to the target and back to the radar. These paths can have path loss variation depending on atmospheric conditions, which produces power fading and enhancement. Path loss variability occurs at longer distances from hour to hour and is characterized with a statistical distribution. The ITS Irregular Terrain Model (ITM) radio wave propagation model is used because it is able to predict power fading and enhancement caused by path loss variability.

Besides establishing IPC, scenario, and models, the previous background report addressed three fundamental interference analysis issues including

- BRS signal characteristics: BRS emissions from a single base station can be reasonably modeled with Gaussian noise. Since its statistics are Gaussian it follows that emissions from an aggregate of base stations will also be Gaussian.

- Aggregate interfering emissions: The interfering signal is the sum of signals from an aggregate of base stations, the mean power and distribution of the aggregate emissions can be determined using ITM and Monte Carlo analysis, and the aggregate emissions from 10 base stations spaced 3 km apart could have as much as 6 dB more power at some distances as compared to a single base station.

- Variable SNR: Interference analysis for scenarios with long radar to target ranges need to account for a variable radar SNR caused by atmospheric conditions that vary from hour to hour. While devising a method for incorporating variable SNR we found that there was a considerable amount of excess power in radar to target link budgets used in acceptance tests. Although this excess SNR could potentially mitigate interference we found that it is needed to accommodate reductions in target mean RCS due to different target aspects, shapes, and materials. We recommended removing the excess power prior to interference analysis by reducing the mean RCS.

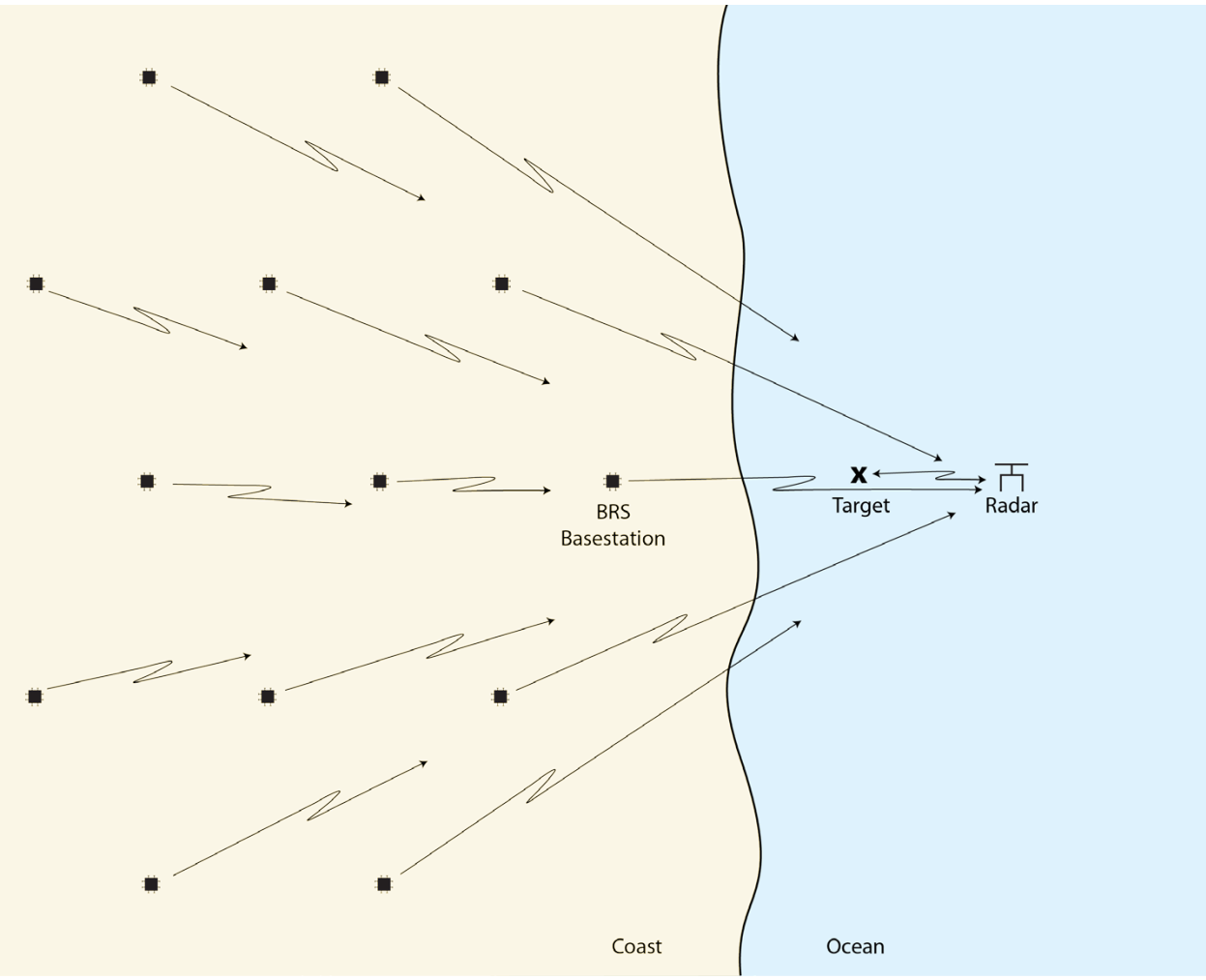

Figure 4. Physical layout showing a network of BRS base stations contributing to the interfering signal power. The interference can cause the radar to not detect the target. Antenna pattern attenuation is not represented in this figure.

1.2 Report Organization

This report determines allowable interference power IPC, front-end filter attenuation, and separation distances needed to prevent overload. The allowable interference power IPC is determined from probability of detection measurements with a custom test fixture. Results are compared to commonly used overload metrics such as receiver front-end gain compression which are easier to execute than probability of detection measurements.

The general problem is discussed in Section 2. Our approach to solving the problem is provided in Section 3. A mathematical description of the method is given in Section 4. A description of the test fixture used in given in Section 5. Results are provided in Section 6. The Appendices provide additional information for the interested reader.

2 FRONT-END OVERLOAD

Front-end overload is caused by strong signals within the radar front-end bandwidth. As an example, the interfering PSD in Figure 5 is within the radar front-end bandwidth and there is potential for front-end overload. In contrast, the interfering PSD in Figure 6 is mostly outside the front-end bandwidth and the potential for front-end overload is greatly reduced.

Front-end overload can be prevented by decreasing the transmitter power, increasing the distance separating the base stations from the radar, and/or increasing the frequency separation between the base station and radar center frequencies. However, the most expedient way to avoid front-end overload is to use a front-end filter whose bandwidth corresponds to the operating band [16]. Then radar signals within the operating band are unattenuated while signals outside the operating band are attenuated. Figure 7 is a general block diagram of the BRS transmitters and radar receiver showing the front-end filter located between the limiter and the low-noise amplifier (LNA) in the radar receiver block. The purpose of this report is to find the front-end filter attenuation needed to prevent overload.

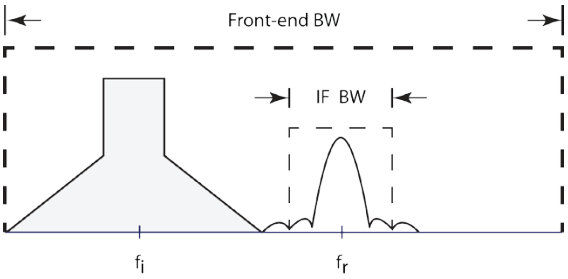

Figure 5. Interfering power spectral density centered at f_i is within the radar front-end bandwidth (BW) (bold outer dashed line). The radar is vulnerable to front-end overload.

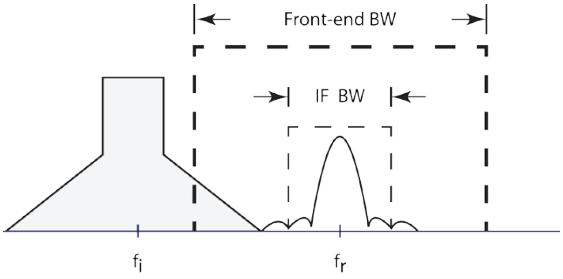

Figure 6. Most of interfering power spectral density centered at f_i is outside of the radar front-end bandwidth (BW) (bold outer dashed line). The radar is protected from front-end overload.

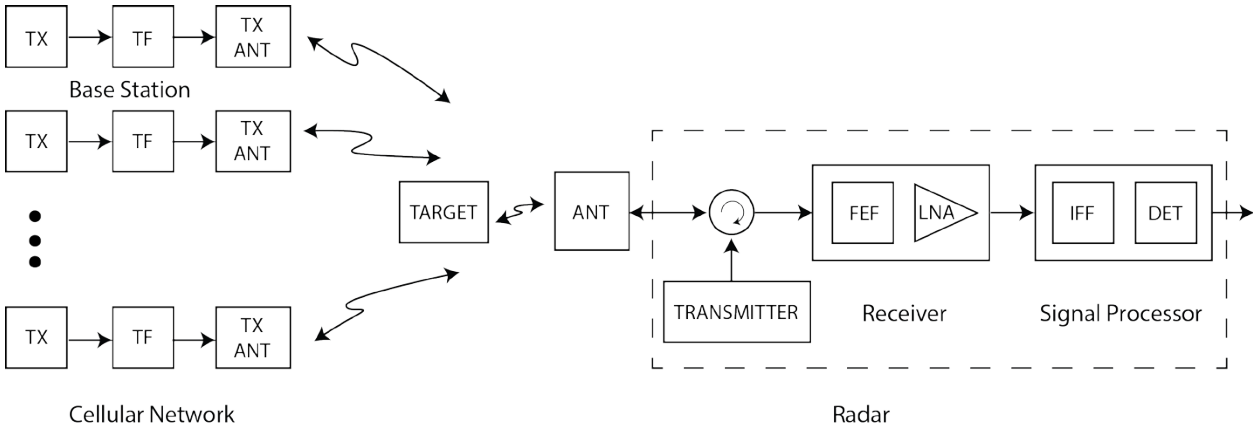

Figure 7. General block diagram of BRS transmitters and radar system. TX represents the transmitter, TF represents the transmitter filter, TX ANT represents the transmitter filter, ANT represents the radar antenna, FEF represents the front-end filter which prevents overload, LNA represents the low-noise amplifier, IFF represents the IF filter, and DET represents the threshold detector.

3 METHOD

The method described here provides a direct measurement of the effect of overload on probability of detection, P_d. The results are used to determine the allowable interference power and the amount of front-end attenuation needed for a specified separation distance. Frequency separation is not determined.

3.1 Effects of Front-End Overload on P_d and P_{fa}

Our method measures the effect of front-end overload on P_d using the amplitude probability distribution (APD) of the voltages present at the radar detector. The APD characterizes the probability that the amplitude of a random signal, A, will exceed a voltage, y

$$Pr\{A > y\} \tag{1}$$

and is typically plotted on a Rayleigh graph whose y-axis or ordinate is scaled so the APD of complex Gaussian noise is represented by a straight, negatively-sloped line with mean power at approximately the 37th percentile [17],[18].

Figures 8 and 9 are renditions of how overload from interference can change the shape of noise and signal plus noise APDs. Actual measurements are shown in Appendix A.

Figure 8 shows the APDs in the absence of the interfering signal. The noise APD determines the threshold voltage, V_T, corresponding to the probability of false alarm, P_{fa}. The P_d is the signal plus noise APD probability corresponding to V_T. In this case the P_d is 0.8 and the P_{fa} is $1x10^{-4}$ or 0.01%.

Figure 9 shows these same APDs when an interfering signal that causes overload is present. The noise curve departs significantly from the straight noise curve in Figure 8 and its mean is elevated. Together these effects require an increase in V_T to maintain the same P_{fa} it had without interference. This in turn lowers the P_d.

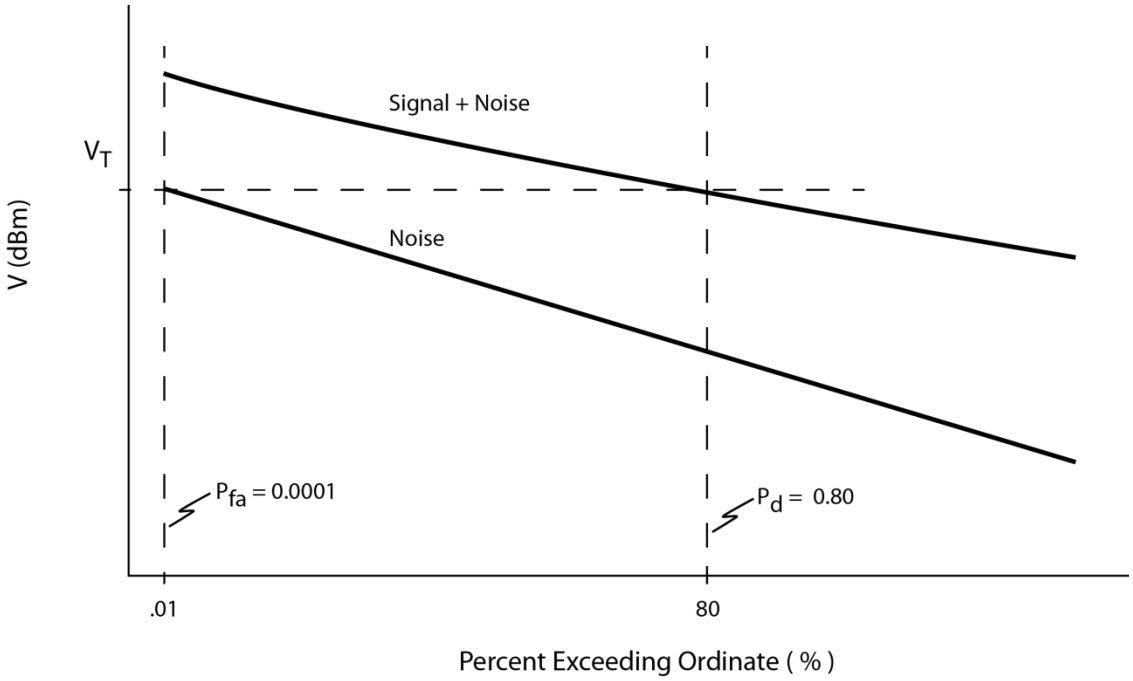

Figure 8. APD of voltages present at the detector when the interfering signal is absent.

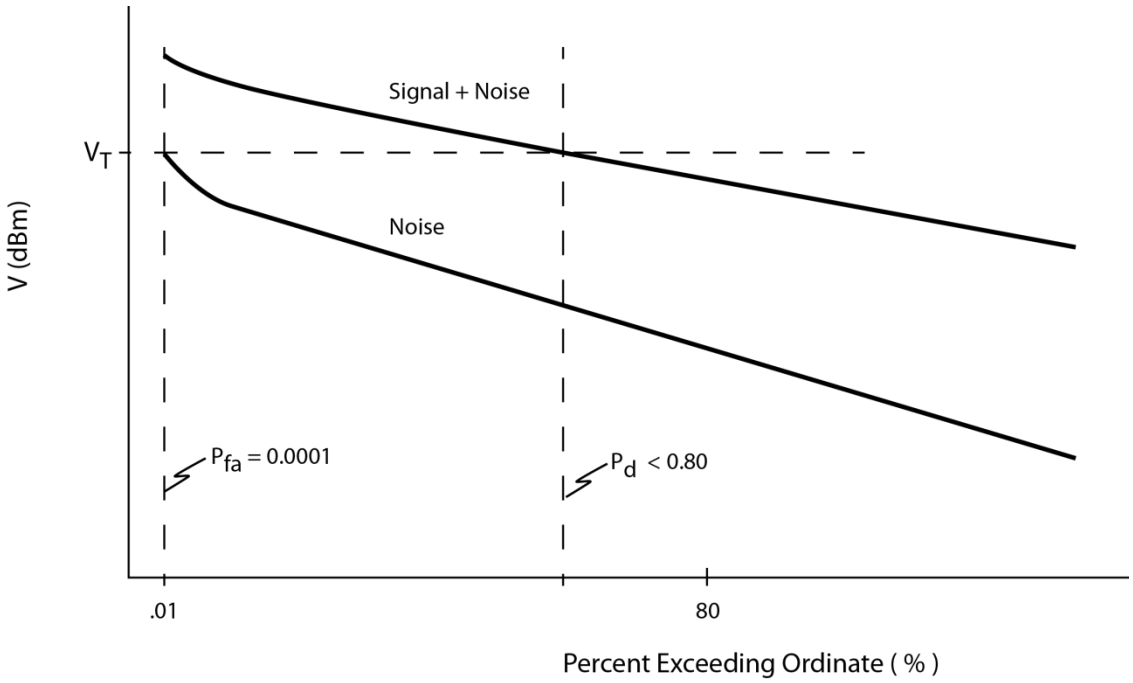

Figure 9. APD of voltages present at the detector when the interfering signal is present.

Front-end overload effects in amplifiers such as gain compression and changes in noise statistics are well understood when the interfering and desired signals are continuous waves (CW) [19], [20]. Briefly, gain compression is caused by a third order non-linearity which shifts power to intermodulation signal components outside the detection bandwidth. The changes in the noise

statistics are caused by a second order non-linearity which shifts low frequency noise to the receiver's center frequency.

The effects are more difficult to analyze when the interfering signal is a random noise process like the BRS signal and there are more electronic circuits than amplifiers involved. In the marine radar there are also circulators, limiters, and mixers that are inherently non-linear devices. Consequently we chose to determine the effect of overload through APD measurement rather than analysis.

3.2 Allowable Interference Power

Interference power, i (or I in dB), is evaluated at the receiver input. The allowable interference power, i_a (or I_a in dB), is the interference power needed to degrade radar performance from baseline to allowable. The allowable interference power is determined by calculating P_d from APD measurements over a range of interference powers. An example of a set of these measurements, referred to as the degradation point (DP) measurement, is shown in Figure 10.

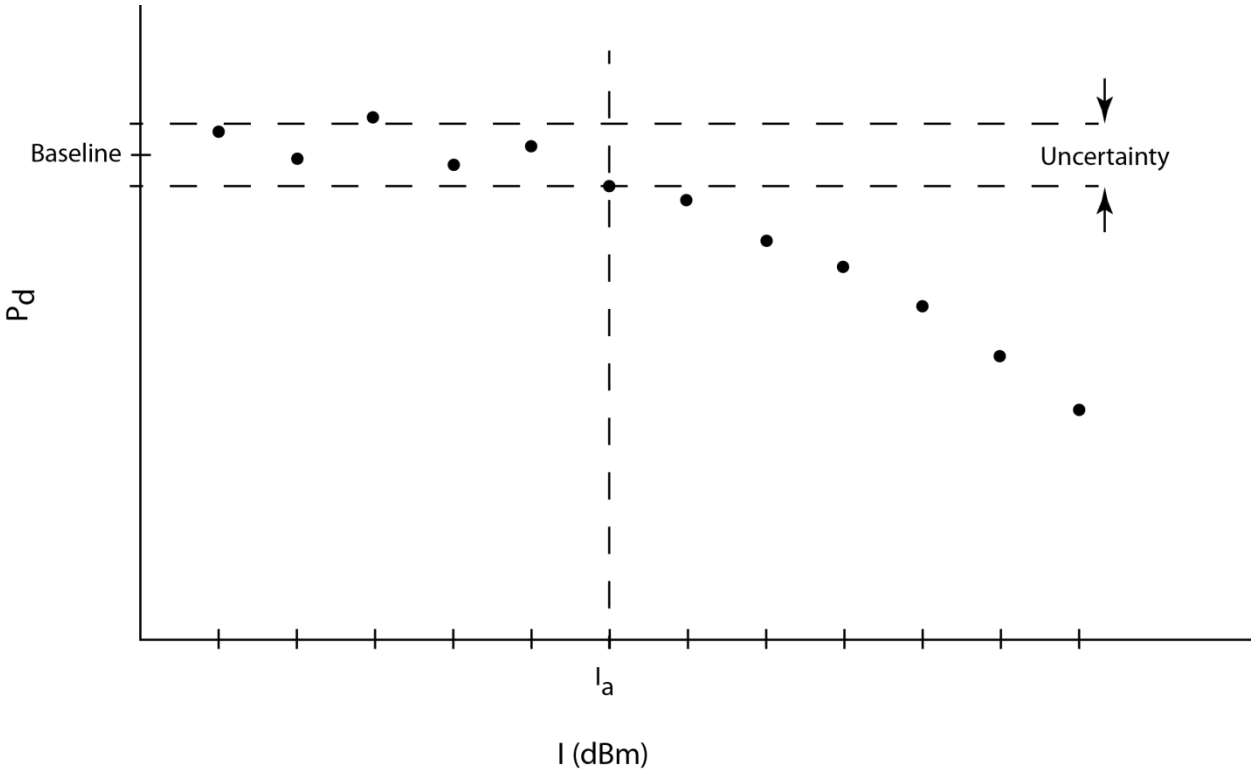

Figure 10. P_d over a range of interfering signal powers.

We assume front-end overload is most likely to occur at short radar-to-target ranges where propagation path loss variability is negligible and SNR and INR are constant as discussed in the previous background report [15]. Consequently, most of the variability is due to RCS fluctuation and experimental uncertainty is dependent on the number of RCS fluctuations measured. Our goal is to use enough fluctuations to detect 5% P_d degradation corresponding to a -6 dB INR for

unwanted emissions. Using Monte Carlo simulation, described in Appendix B, we determined that approximately 400 fluctuations were needed.

Figure 11 is a flow chart of the sequence of steps for this measurement. Briefly, the sequence turns off the radar signal, S; sets the interfering signal power, I; collects noise data; and determines the V_T for the desired P_{fa} from the noise APD. It then turns the radar signal on; calculates a realization of the Swerling 1 RCS fluctuation factor, k; sets the radar signal level to the product of k and the baseline SNR; collects signal plus noise data; and determines the P_d corresponding to V_T from the signal plus noise APD. This is done a number of times with new RCS fluctuation factor realizations to reduce uncertainty. The set of P_d is then averaged. Mathematical details are provided in Sections 4.2 and 4.1.

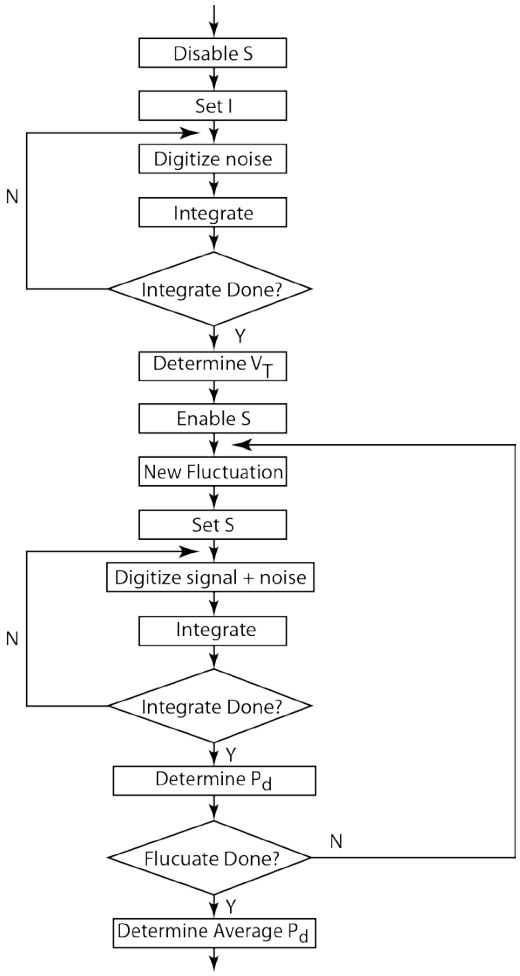

Figure 11. Flow chart showing sequence of measurement and data processing steps.

3.3 Separation Distance and Front-End Filter Attenuation

Following the derivation in the previous background report [15], the link budget equation for the aggregate interfering signal power at the radar receiver is

$$i(d_1) = \sum_{n=1}^{N} i_{single}(d_n) = \sum_{n=1}^{N} \frac{\hat{p}_{ta}\hat{g}_t g}{\sqrt{l_d l_{bm}}\, l_{pol} l_{cr}} \cdot \frac{1}{\tilde{l}_{p,n}(d_n)} \quad (2)$$

where i_{single} is the interfering signal power from a single base station, d_1 is the distance from the radar to the closest base station, d_n is the distance from the n-th base station to the radar, N is the number of base stations in the aggregate, $\hat{p}_{ta}$ is the signal power at the transmit antenna, $\hat{g}_t$ is the gain of the base station antenna in the direction of the radar, g is the gain of the radar antenna in the direction of the base station, l_d is the radome loss, l_{bm} is the integration beam shape loss, l_{pol} is the polarization loss between the base station and radar antennas, l_{cr} is the radar receiver circuit loss, and $\tilde{l}_{p,n}$ is the path loss from the n-th base station to the radar.

Finally, the front-end filter attenuation required is

$$L_{FE}(d_1) = I(d_1) - I_a \ (dB) \quad (3)$$

4 MATHEMATICAL FOUNDATIONS

4.1 Target RCS Fluctuation

Radar power returned from one target RCS fluctuation realization can be obtained using the method of uniform deviates. The Swerling 1 radar cross section density function is exponential

$$f(\sigma) = \frac{1}{\sigma_{av}} e^{-\sigma/\sigma_{av}}, \qquad \sigma > 0 \tag{1}$$

with mean σ_{av} and variance σ_{av}^2. Its corresponding distribution is

$$F(\sigma) = Pr\{\Sigma < \sigma\} = \int_0^{\sigma} \frac{1}{\sigma_{av}} e^{-x/\sigma_{av}} dx = 1 - e^{-\sigma/\sigma_{av}} \tag{2}$$

The density function for the uniform distribution is

$$f(u) = \begin{cases} \dfrac{1}{b-a}, & a \le u \le b \\ 0, & elsewhere \end{cases} \tag{3}$$

and its corresponding distribution function is

$$G(u) = Pr\{U < u\} = \int_0^{u} dx = u \tag{4}$$

when $b = 1$, $a = 0$, and $0 \le u \le 1$.

Setting

$$Pr\{\Sigma < \sigma\} = Pr\{U < u\} \tag{5}$$

then

$$1 - e^{-\sigma/\sigma_{av}} = u \tag{6}$$

$$k = \frac{\sigma}{\sigma_{av}} = -\ln(1-u) \tag{7}$$

and the power of j-th radar cross section realization is

$$p_{s,j} = p_s k_j \tag{8}$$

where p_s is the mean power.

4.2 Interference Measurement Data Processing

4.2.1 Noise Measurement Data Processing

Noise data processing determines the threshold voltage, V_T. The noise record consists of measurement samples

$$n_j, \qquad j = 1, \ldots J \tag{4}$$

where j is the measurement sample index and J is the number of samples. The non-coherently integrated noise envelope is computed from K noise records by

$$\eta_j = \sum_{k=1}^{K} |n_{j,k}| \tag{5}$$

where k is the integration index and K is the number of integrations.

The noise APD , $Pr\{\eta_j > v\}$, estimate is created by sorting the integrated noise from high to low into the vector V where

$$V[1] > V[2] > \cdots > V[J] \tag{6}$$

and pairing the sorted data with probabilities from $1/J$ to 1.0. The voltage threshold is

$$V_T = V[m] \tag{7}$$

where

$$m = \lfloor P_{fa} * J \rfloor \tag{8}$$

and $\lfloor \cdot \rfloor$ is the rounding-down or floor operator.

4.2.2 Received Signal Data Processing

Received signal data processing determines the P_d. The received signal is $r = s + n$. The received signal record consists of measurement samples

$$r_j, \qquad j = 1, \ldots J \tag{9}$$

where j is the measurement sample index and J is the number of samples. The non-coherently integrated received signal envelope is computed from K noise records by

$$\rho_j = \sum_{k=1}^{K} |r_{j,k}| \tag{10}$$

where k is the integration index and K is the number of integrations.

The received signal APD, $Pr\{\rho_j > y\}$, estimate is created by sorting the integrated data from high to low into the vector V where

$$V[1] > V[2] > \cdots > V[J] \tag{11}$$

and pairing the sorted data with probabilities from $1/J$ to 1.0. The probability of detection is

$$P_d = m/J \tag{12}$$

where m is the largest integer that satisfies

$$V[m] > V_T \tag{13}$$

The P_d averaged over all the target RCS fluctuation realizations is

$$P_d = \frac{1}{L}\sum_{l=1}^{L} P_{d,l} \tag{14}$$

where l is the fluctuation index and L is the number of fluctuations.

4.2.3 Power and Power Ratios

The noise power is

$$p_n = \frac{1}{J}\sum_{j=1}^{J} |n_j|^2 \tag{15}$$

The signal plus noise power is

$$p_r = \frac{1}{J}\sum_{j=1}^{J} |r_j|^2 \tag{16}$$

The signal to noise ratio is

$$\gamma = \frac{p_r - p_n}{p_n} \tag{17}$$

The average SNR over all fluctuations is

$$\gamma = \frac{1}{L}\sum_{l=1}^{L}\gamma_l \tag{18}$$

where l is the fluctuation index and L is the maximum number of fluctuations.

5 FRONT-END OVERLOAD TEST FIXTURE

The block diagram in Figure 12 shows key components for analyzing front-end overload. The low-noise amplifier (LNA) is considered the most vulnerable to overload. However the circulator and limiter are non-linear devices and can also overload. The antenna, circulator, and limiter provide some degree of protection to the LNA because of their bandwidth limitations. The front-end filter (FEF) provides the rest.

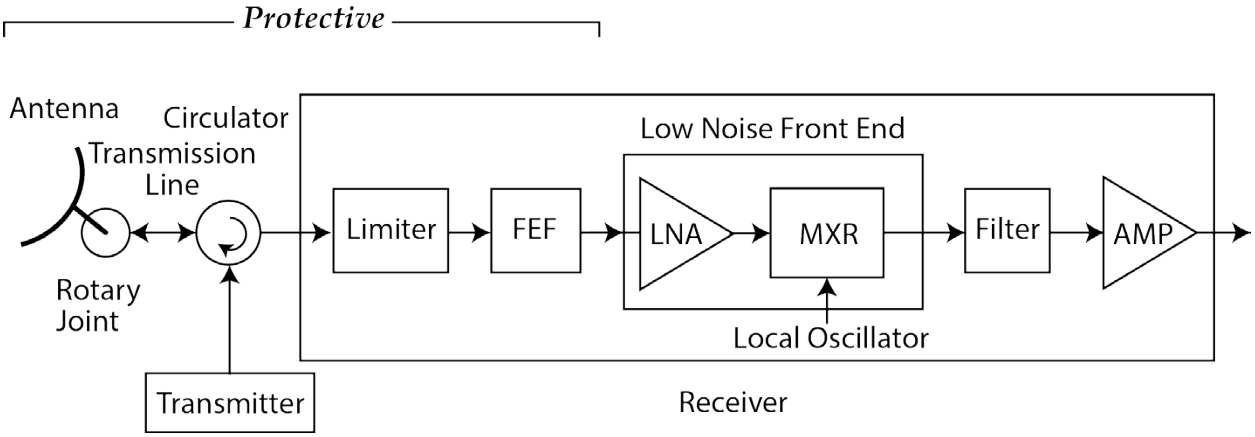

Figure 12. Radar system block diagram showing key components for analyzing front-end overload. FEF represents the front-end filter, LNA represents the low-noise amplifier, MXR represents the mixer, and AMP represents the amplifier.

Figures 13 and 14 show a block diagram and a photograph of the test fixture. The aggregate BRS signal is emulated with band limited Gaussian noise created by a vector signal generator (VSG). The BPF at the output of the VSG attenuates its spurious emissions so they are insignificant in the radar bandwidth. The radar signal is emulated by a 3050 MHz CW signal created by a signal generator (SG). In using a CW signal, we are assuming that the front-end overload does not distort the radar pulse shape. These two signals are combined and applied to the radar front-end which is placed inside a metal box to reduce noise.

The second signal generator (LO) supplies the 3110 MHz local oscillator signal to the front-end. The front-end output is applied to the 60 MHz center-frequency IF section which prepares the signal for the vector signal analyzer (VSA), spectrum analyzer (SA), and power meter (PM) data collection instruments. For the interested reader, test fixture schematics and specifications are provided in Appendix C.

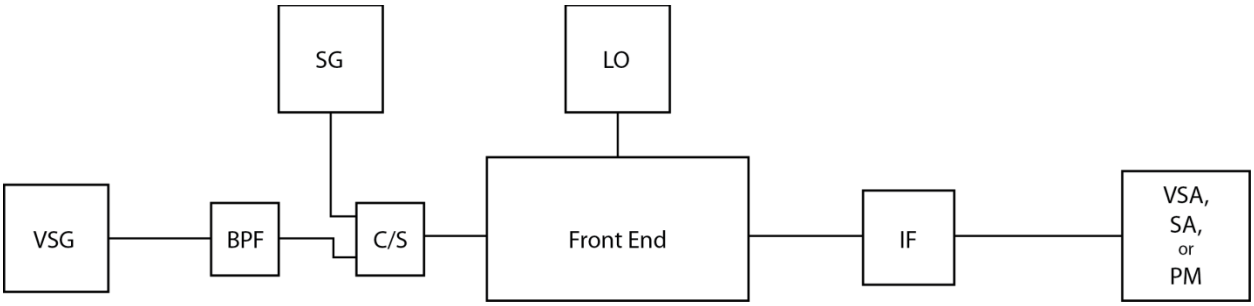

Figure 13. Front-end overload test fixture block diagram. From left to right are the vector signal generator (VSG), band pass filter (BPF), radar signal generator (SG), combiner/splitter (C/S), front-end, local oscillator (LO), intermediate frequency section (IF), and the test instruments including the vector signal analyzer (VSA), spectrum analyzer (SA), and the power meter (PM).

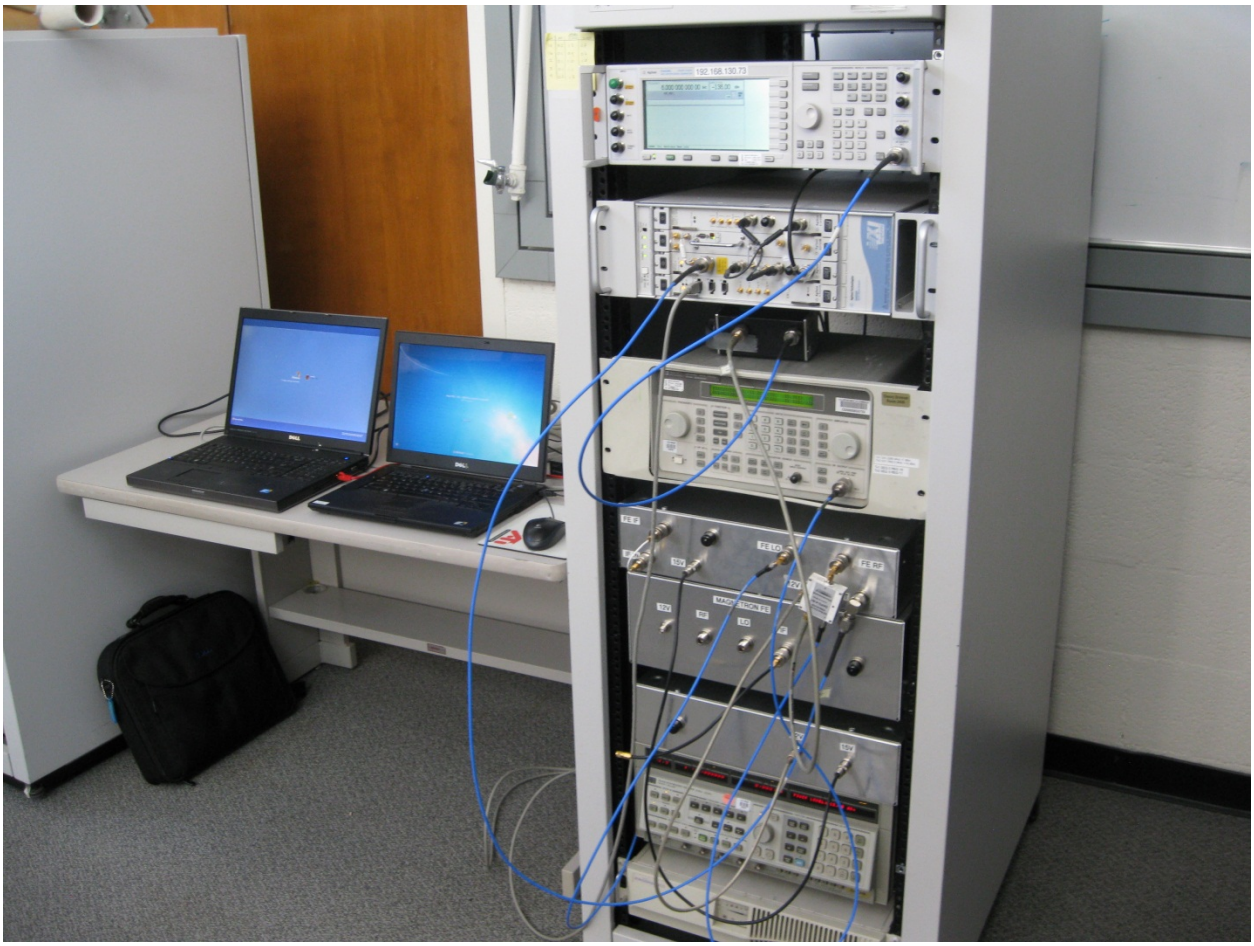

Figure 14. Front-end overload test fixture. From top to bottom in the rack are the vector signal generator (VSG), vector signal analyzer (VSA), band-pass filter (BPF) (small black box), radar signal generator (SG), reference front-end and IF section, magnetron front-end assembly, power supplies, local oscillator (LO), and power conditioning unit.

5.1 Front-end

Figures 15 and 16 are a photograph and block diagram, respectively, of the magnetron front-end assembly used in the test fixture. The assembly consists of a circulator, limiter, and LNFE—all commercial off-the-shelf components. A terminator replaces the radar transmitter. The terminator, circulator, and limiter are waveguide components.

Figure 17 is a block diagram of the LNFE, which consists of a low-noise amplifier (LNA) and a two-mixer, image-rejection, frequency down-conversion circuit. The LNFE was modified by the manufacturer to accept an external local oscillator signal so that all front-ends could use the same local oscillator.

The magnetron front-end assembly LNFE is sealed and characteristics of the components in it are unknown. Consequently, we also chose to design and build what we refer to as a reference front-end from discrete components whose characteristics are known. The reference front-end does not have the filtering by the circulator and limiter that the magnetron front-end assembly has. A photograph of the reference front-end is shown in Figure 18. The reference front-end block diagram is identical to that of the magnetron front-end assembly LNFE in Figure 17.

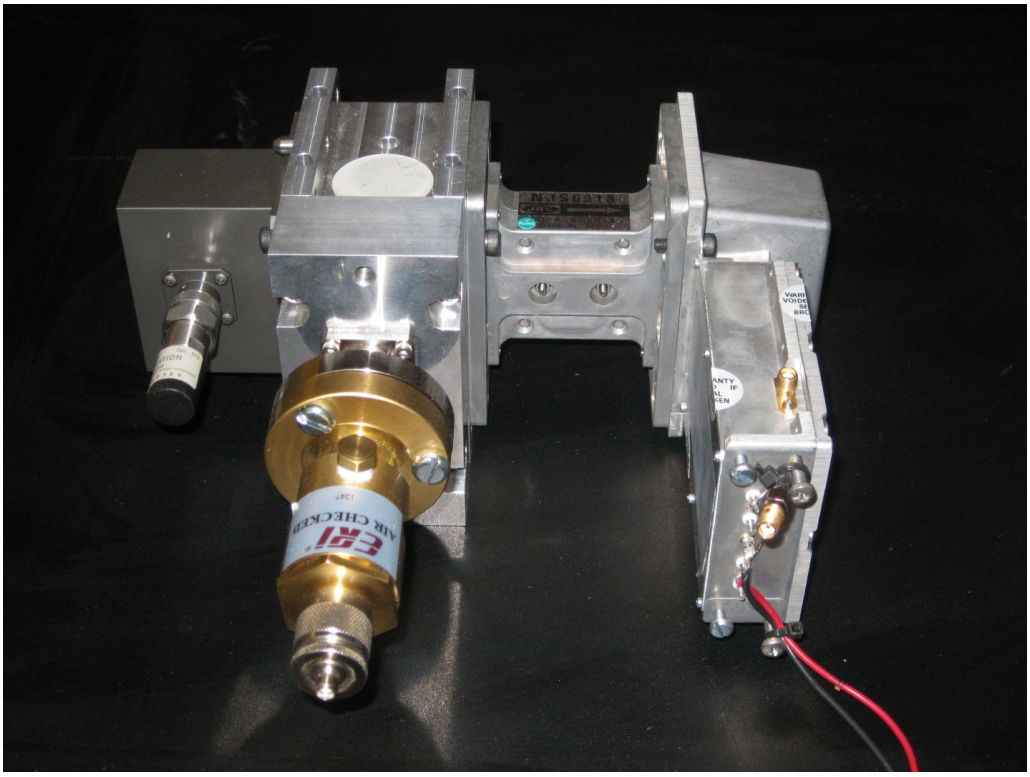

Figure 15. Magnetron front-end assembly. Components (from left to right) are waveguide terminator, circulator, limiter, and low-noise front-end. The signal and interference are applied at the SMA to type-N adaptor on the circulator. The local oscillator signal from the signal generator is applied to the SMA connector on top of the LNFE. The IF signal is taken from the SMA connector on the side of the LNFE.

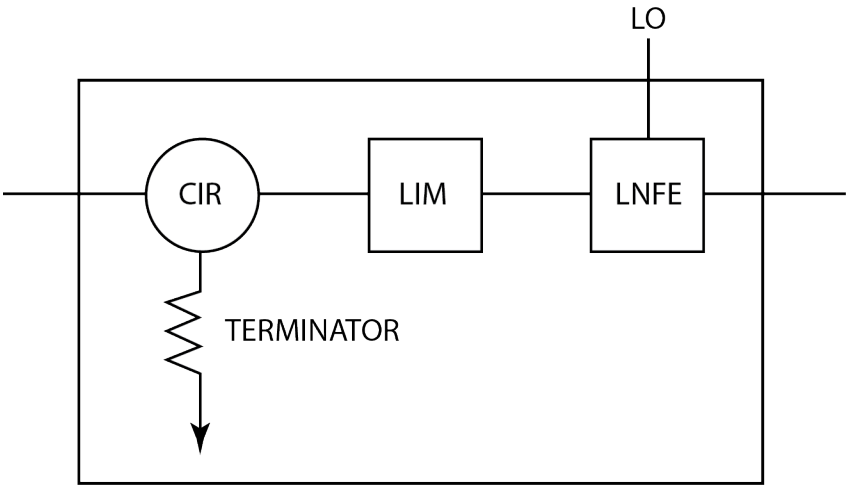

Figure 16. Magnetron radar front-end assembly block diagram. CIR represents the circulator, LIM represents the limiter, and LNFE represents the low-noise front-end.

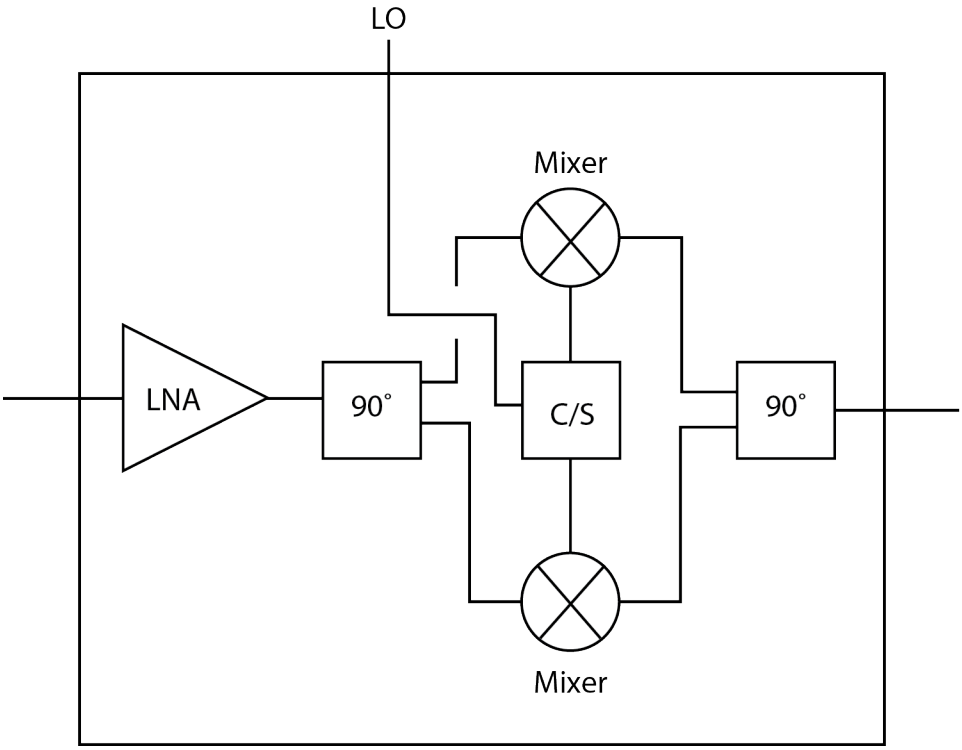

Figure 17. Low-noise front-end block diagram. LNA represents the low-noise amplifier, C/S represents the combiner/splitter, circle with a cross represents a mixer, and the block with 90^{o} represents the quadrature combiners/splitters.

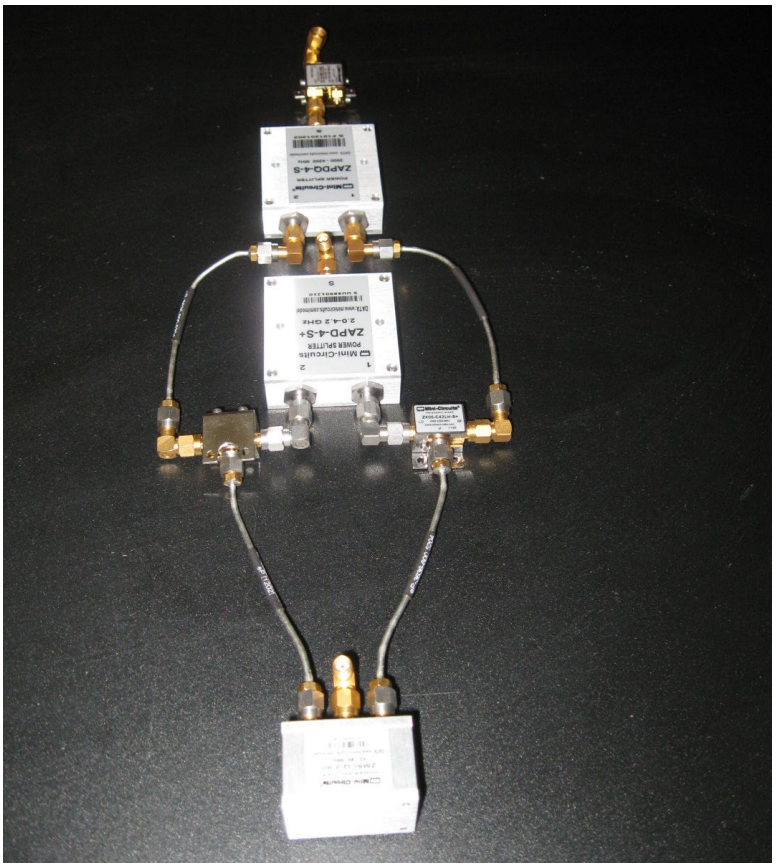

Figure 18. Reference front-end. Components (from top to bottom) are the LNA, quadrature splitter, splitter, mixers, and quadrature combiner. The signal and interference are applied to the LNA input, the local oscillator signal is applied to the splitter, and the IF signal is taken from the quadrature combiner.

5.2 Test Fixture Characterization

Test fixture gain, gain compression, and noise figure measurements were made to characterize its operation under normal operation conditions. Procedures for these measurements can be found in Appendix D and Appendix E. Comprehensive results using the procedures are presented in Appendix F. This section contains highlights of front-end and emulated BRS signal characterization results.

5.2.1 Front-end Characterization

Circulator and limiter frequency responses measured with a VNA are shown in Figure 19. The least attenuation is over the 2900–3100 MHz marine radar band. When combined, the circulator and limiter have an approximately 500 MHz 3 dB bandwidth beginning at 2700 MHz and ending at 3200 MHz. Outside this range, limiter attenuation increases steeply as compared to the circulator. The circulator has a deep null around 2850 MHz.

Front-end gain was measured with a 3050 MHz CW signal in the center of the radar detection bandwidth with a power that would not cause overload. Front-end gain compression was measured in the same way, with the exception that the power was increased to the 1 dB gain compression point (GCP). The 1 dB GCP is the minimum amount of power at which a 1 dB increase in input power produces no measurable increase in output power.

Noise powers were too low to be measured without gain from the IF section so they were calculated from the system and IF section noise figures. The noise figures were measured using the Y-factor method with a noise diode source. With the Y-factor method, noise figure is computed from two measurements, with the noise diode turned off and then on.

Figure 20 shows the results of the gain compression measurement. The gain compression curves of the reference front-end and magnetron front-end assembly are practically identical. The 1 dB GCPs for the reference front-end and magnetron front-end assembly are approximately 2 and 1 dBm, respectively.

Results for all the characterization measurements are summarized in Table 1. These results show that the reference front-end and magnetron front-end assembly have similar characteristics.

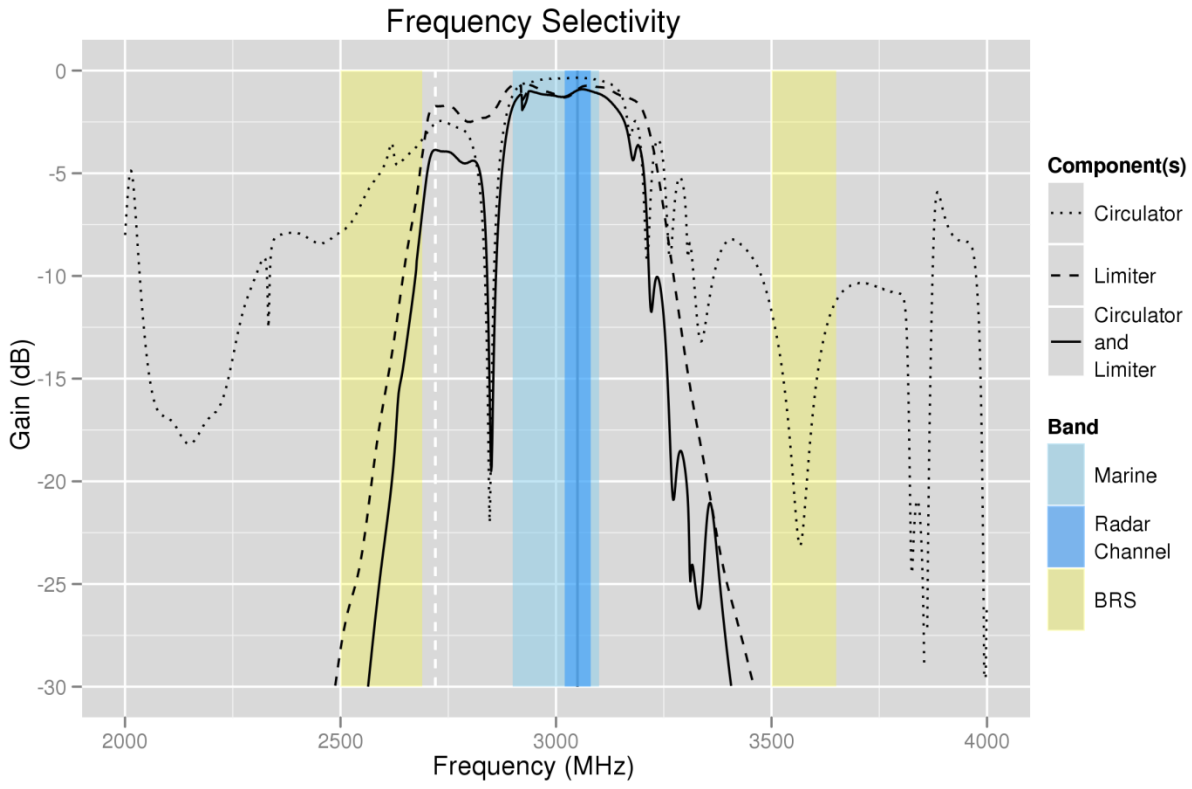

Figure 19. Frequency selectivity for circulator, limiter, and their combination. The marine radar band extends from 2900-3100 MHz. The radar channel is 60 MHz wide and centered at 3050 MHz. The interfering BRS signal was tuned to 2720 MHz as indicated by the white dashed line. The 2500-2690 MHz band is currently used for BRS. The 3500-3650 MHz band is being evaluated.

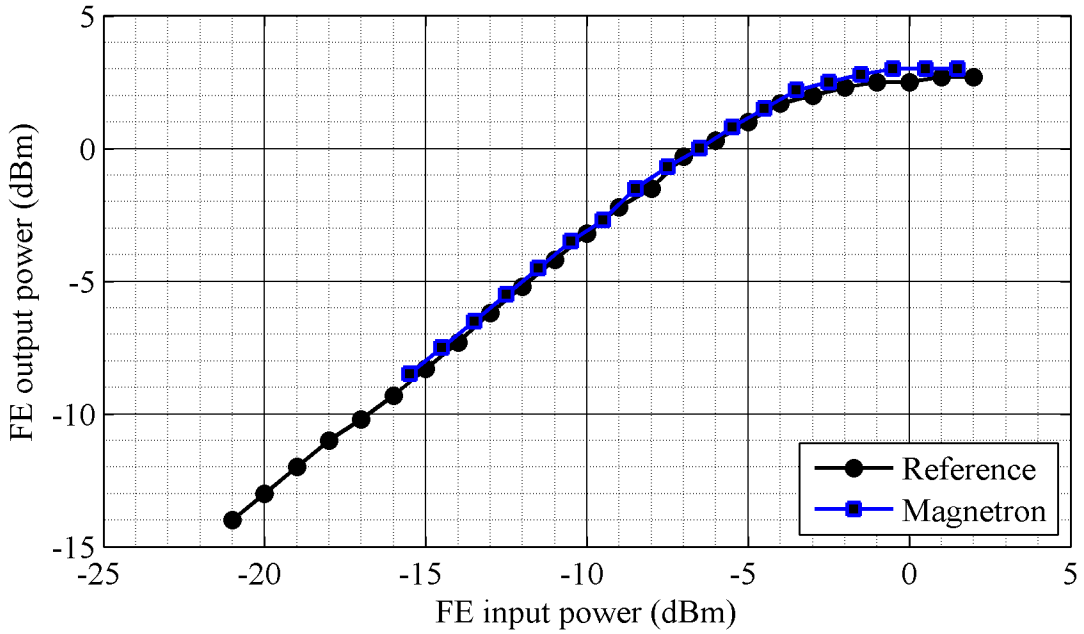

Figure 20. Front-end gain compression curves.

Table 1. Gain and noise figure measurement results.

	Gain (dB)	Input 1 dB GCP (dBm)	Noise Figure (dB)	Notes
Reference front-end	5.8	2	5.0*	* Calculated
Magnetron front-end assembly	6.5	1	5.3*	* Calculated

5.2.2 BRS Signal Characterization

The BRS signal is emulated by a 10 MHz wide Gaussian noise signal. The duration of the emulated signal exceeds the length of time used to collect one APD measurement. The signal begins as a 100 MHz Gaussian noise complex baseband signal. It is then filtered by a 256 tap 10 MHz bandwidth FIR filter, converted to the VSG format, and loaded into the VSG for playback. The VSG shifts the complex baseband signal to the interfering signal center frequency.

The ideal interfering signal frequency would have little circulator and limiter attenuation and a large frequency offset from the marine radar band. A large frequency offset is needed so that VSG spurious responses can be filtered out before they enter the radar detection bandwidth. Figure 19 in the previous section showed 2720 MHz met these qualifications. Hence, we used 2720 MHz for the interfering signal frequency.

Figure 21 shows the power spectral density (PSD) of the emulated BRS signal at complex baseband centered at 0 Hz. The PSD was created by the Welch method using 128 blocks of 131,072 samples. The Hamming window was used to reduce spectral leakage. The emulated

signal occupies approximately 10 MHz from -5 MHz to 5 MHz. The frequency increment is 763 Hz.

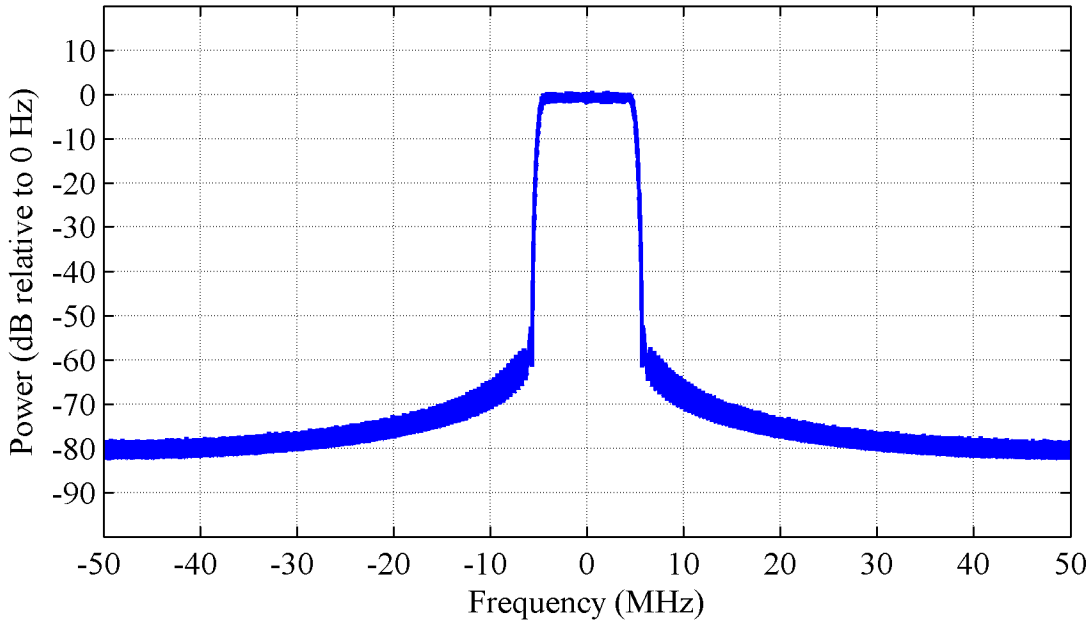

Figure 21. Power spectral density of emulated BRS signal.

5.3 Instrument Control and Data Processing

Instrument control and data processing tasks were performed with a software algorithm and computer. Instrument control consisted primarily of setting VSG and SG powers corresponding to interference and radar powers and digitizing signals with the VSA. Details regarding instrument control are provided in Appendix G. Data processing consisted of integrating data, constructing APDS from the integrated data, and calculating V_T and P_d, from the APDs.

6 RESULTS

6.1 Parameters

Parameters for the physical layout, radar, radio wave propagation, target, and BRS system are provided in the previous background report [15]. Table 2 summarizes relevant radar and BRS parameters.

Table 2. Radar and BRS parameters used for analysis.

Parameter	Value	Note
$\hat{p}_{ta}$	13.0 dBW	20 W for 10 MHz channel at antenna
$\hat{g}_t$	15 dB	
g	27.0 dB	
l_d	1.0 dB	Two-way
l_{bm}	1.6 dB	Two-way
l_{sp}	0.0 dB	
l_{cr}	2.7 dB	
l_{ct}	2.7 dB	
l_{pol}	3.0 dB	Radar is horizontally polarized. BRS is 45 degree slant cross polarized.

6.2 IPC

Relevant IPC parameters are summarized in Table 3. The baseline SNR is determined without signal processing loss. Signal processing loss caused by imperfect matched filtering, sampling, and CFAR is not applicable to this experiment, where a CW radar signal is used and the threshold is set during analysis.

Tests were conducted with and without pulse integration. With no integration, the baseline SNR is 10.98 and 16.05 dB for Swerling 0 (no target fluctuations) and 1 (target fluctuations), respectively. Tests with integration used the IEC 62388 long and short pulses at a 40 rpm antenna rotation rate. Relevant pulse parameters and baseline SNR are provided in Table 4. More detailed information regarding the IEC 62388 pulses can be found in the previous background report [15].

Table 3. IPC parameters.

IPC	Value	Note
Baseline performance	0.8 $\mathcal{P}_d$ at 10^{-4} P_{fa}	IEC 62388 clear air, calm sea standard
Allowable performance degradation	0.76 $\mathcal{P}_d$ at 10^{-4} P_{fa}	5% DP
Reliability	90%	

Table 4. Baseline SNR for a 1.9 degree beam-width antenna at baseline performance 0.8 P_d and 10^{-4} P_{fa}. PW is pulse width, PRF is pulse repetition frequency, BW is IF filter bandwidth, RR is rotation rate, and n_p is the number of pulses integrated.

Pulse	PW (ns)	PRF (Hz)	BW (MHz)	RR (rpm)	n_p	Baseline SNR (dB)	
						Swerling 0	Swerling 1
Short	50	1800	20	40	14	2.31	7.58
Long	800	785	3	40	6	4.83	10.03

6.3 Preliminary Parameter Study

Effects of radar receiver bandwidth and integration were evaluated to determine how sensitive I_a is to pulse parameters in Table 4. The effect of interfering signal characteristics were also studied. The nominal measurement to which all others were compared was executed with the reference front-end, no target fluctuations (Swerling 0), no integration, 10 MHz bandwidth limited Gaussian noise centered at 2720 MHz, and a 4.6386 MHz radar receiver bandwidth.

The effect of receiver bandwidth was evaluated by doubling the receiver bandwidth to 9.2773 MHz. The effect of integration was evaluated by increasing the number of pulses integrated to 6 and then 14. The effect of signal characteristics was evaluated by replacing the Gaussian noise with a CW signal at the same frequency.

Results of these experiments are shown in Figures 22 and 23. Doubling the radar bandwidth to 9.2773 MHz and increasing pulse integration had no significant effect on I_a. Hence it is unlikely that our results will be dependent on the pulse in Table 4 we choose to emulate. Consequently, integration levels higher than 6 were not measured due to measurement time constraints. The results also show that the CW signal I_a is approximately 3 dB more than the I_a for the 10 MHz bandwidth limited Gaussian noise. Consequently, I_a is sensitive to signal statistics and it is important to do the tests with the emulated BRS signal.

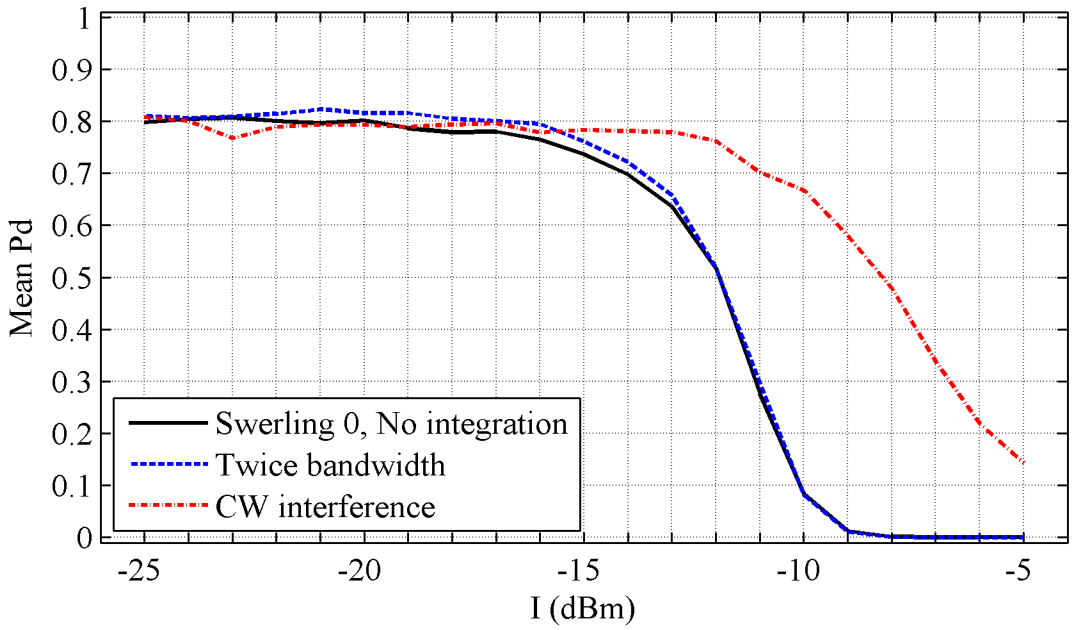

Figure 22. Effect of radar receiver bandwidth and continuous wave (CW) interference on reference front-end performance degradation.

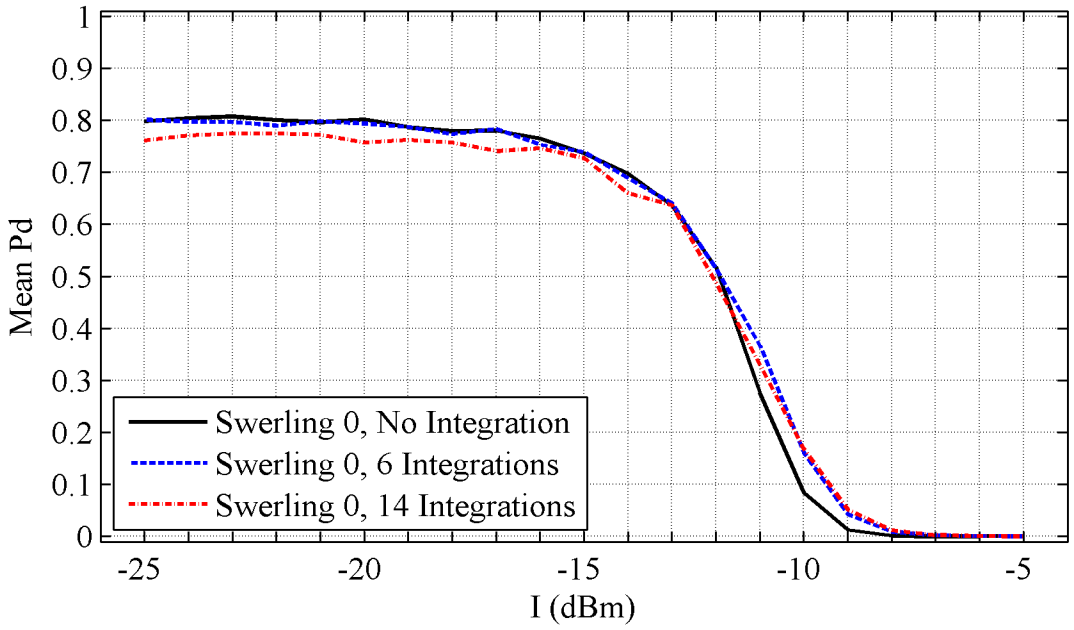

Figure 23. Effect of pulse integration on reference front-end performance degradation.

6.4 Allowable Interference Power

Figures 24 and 25 show performance degradation for both front-ends, Swerling 0 and Swerling 1 fluctuations, without integration, and with 6 integrated pulses. Figure 26 highlights the Swerling 1 fluctuation, 6 integrated pulses results from which we will obtain the I_a needed to estimate the minimum amount of front-end attenuation. These results show that the 5% DP I_a is approximately -11.5 and -9 dBm for the reference front-end and magnetron front-end assembly, respectively.

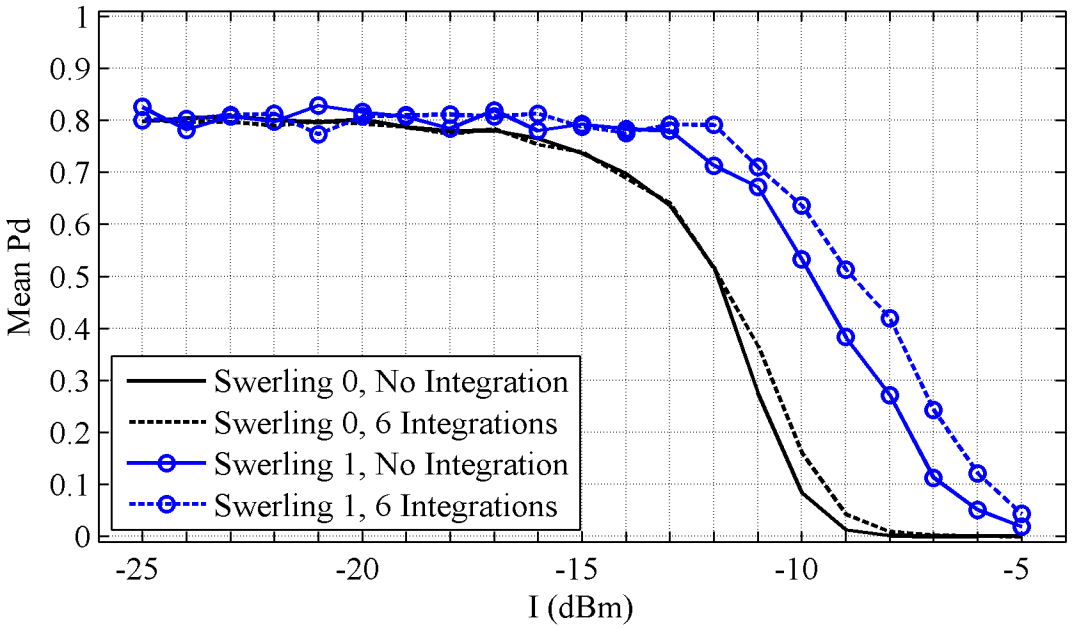

Figure 24. Effect of Swerling model and integration on reference front-end performance degradation.

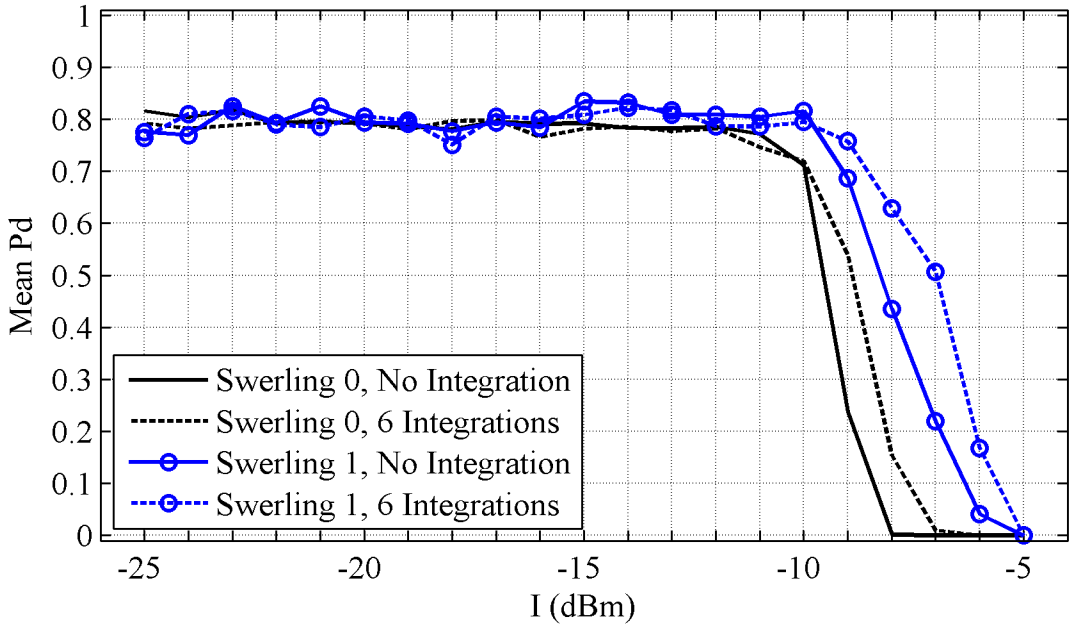

Figure 25. Effect of Swerling model and integration on magnetron front-end degradation.

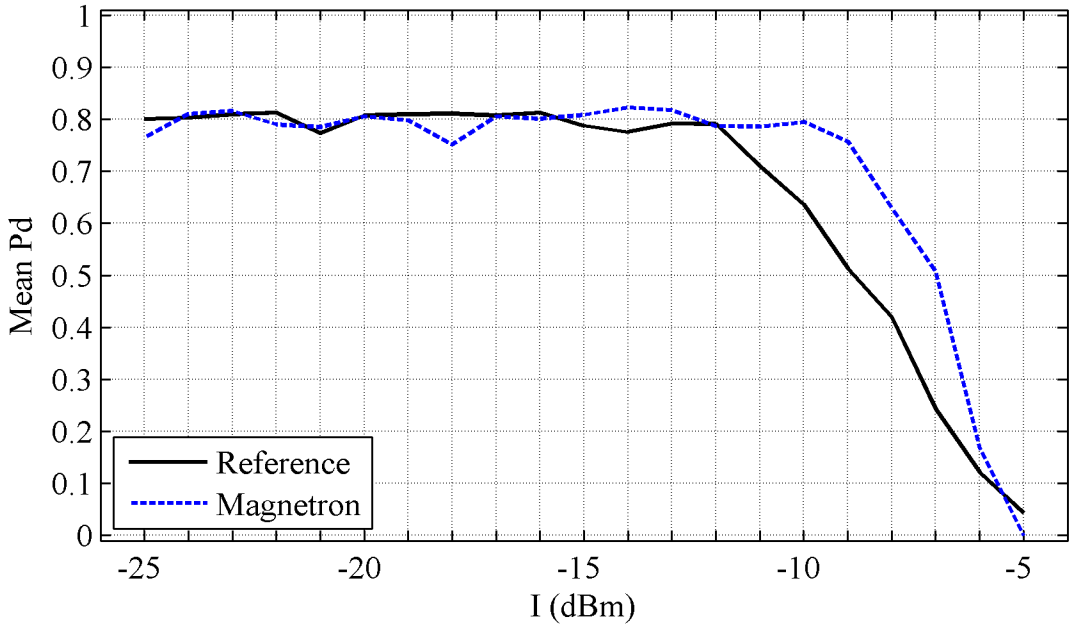

Figure 26. Reference and magnetron front-end performance degradation for Swerling 1, 6 integrations.

6.5 Aggregate Emissions

Figure 27 shows the aggregate emission power with respect to the distance to the closest base station, d_1. Power at distances over 1 km is calculated with the ITM [21]. Power at distances below 1 km but above the minimum far field distance is calculated with free space loss. The minimum far field distance is

$$d_{ff} = \frac{2d_{ap}^2}{\lambda} \tag{19}$$

where d_{ap} is the antenna maximum aperture and λ is the wavelength. This expression is valid when $d_{ap} > 1.5\lambda$ [22]. When transmit and receive antennas have different apertures the one with the larger aperture will determine the far field distance. Assuming the radar antenna aperture is 4 meters and the BRS antenna aperture is 1.5 meters, d_{ff} would be determined by the radar antenna and is approximately 320 meters at 3 GHz.

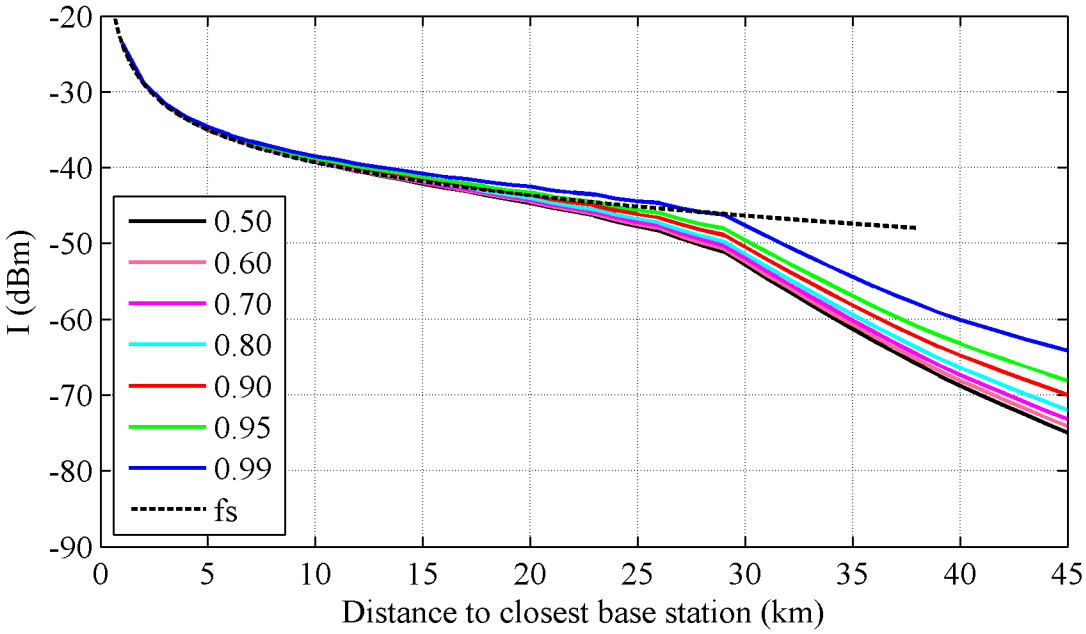

Figure 27. Aggregate interference power versus distance for various probabilities that the interference power (I) is less than the value on the ordinate (y-axis).

6.6 Front-end Attenuation and Separation Distance

Front-end attenuation needed by the reference front-end at different radar to base station separation distances is provided in Table 5. An L_{fe} less than 0 implies that no additional attenuation is needed. The results show that the front-end needs no additional attenuation for distances as close as 400 meters. Since the magnetron front-end assembly I_a is 2.5 dB higher,

this result would be true for the magnetron front-end assembly as well. Results need to be adjusted to accommodate more signals.

Table 5. Filter attenuation required for reference front-end at various distances when the allowable interference power is -11.5 dBm. Negative attenuation corresponds to protection.

Distance (km)	***I* (dBm)**	**L_{FE} (dB)**
1.0	-23.63	-12.13
0.9	-22.71	-11.21
0.8	-21.69	-10.19
0.7	-20.53	-9.03
0.6	-19.19	-7.69
0.5	-17.61	-6.11
0.4	-15.67	-4.17

6.7 Comparison of 5%DP to GCP and NEP

The 5% DP measurement takes a long time. Consequently the 2720 MHz BRS signal 1 dB GCP and 1 dB noise enhancement point (NEP) measurements, which take less time, were performed to see if degradation can be measured in a more timely manner. The 2720 MHz BRS signal 1 dB GCP is the minimum amount of power at which a 1 dB increase in input power produces no measurable increase in output power. The NEP is the minimum amount of input power needed to increase the noise floor by 1 dB. Measurement procedure details are provided in Appendix H. Results for these measurements are shown in Figures 28 and 29. Table 6 compares the results of these measurements along with the in-band 3050 MHz CW 1 dB GCP used to characterize the front-end.

The magnetron 2720 MHz 1-dB GCP is 7 dB less than the 5% DP and therefore a poor predictor of the 5% DP. The in-band 3050 MHz 1-dB GCP was offset 10 or more dB for both front-ends. Furthermore the offset was not consistent. Consequently it is also a poor predictor of the 5% DP. The 1-dB NEP is within 1 dB of the 5% DP for both front-ends and appears to be a good predictor of the 5% DP.

Table 6. Comparison of various performance metrics.

	3050 MHz CW	**2720 MHz BRS**		
Front-end	**1-dB GCP (dBm)**	**1-dB GCP (dBm)**	**1-dB NEP (dBm)**	**5%DP (dBm)**
Reference	2	-10.5	-11.5	-11.5
Magnetron	1	-2	-8	-9

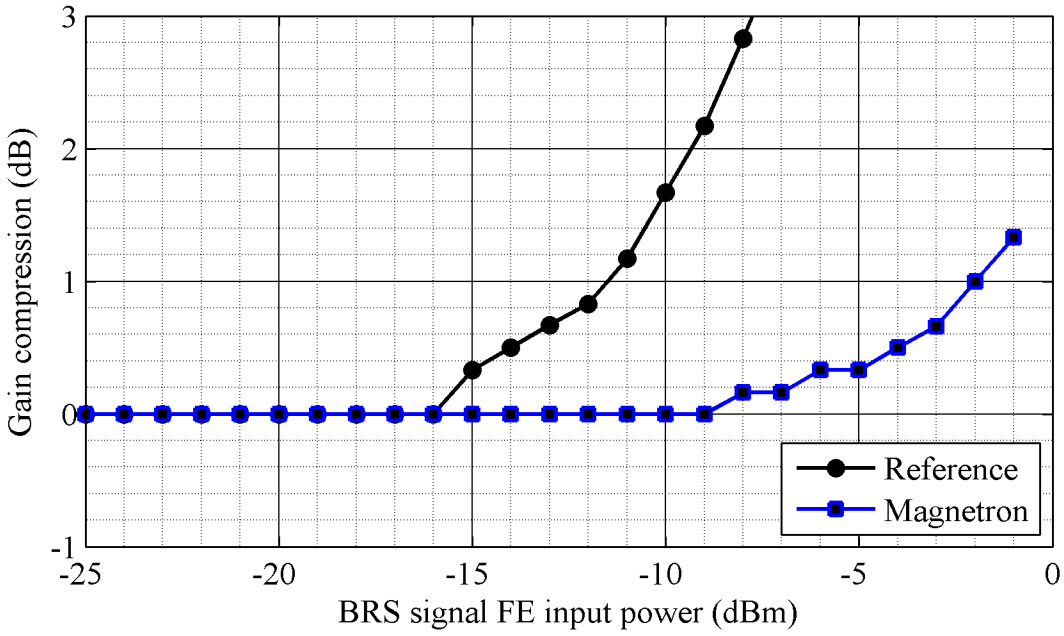

Figure 28. System gain compression.

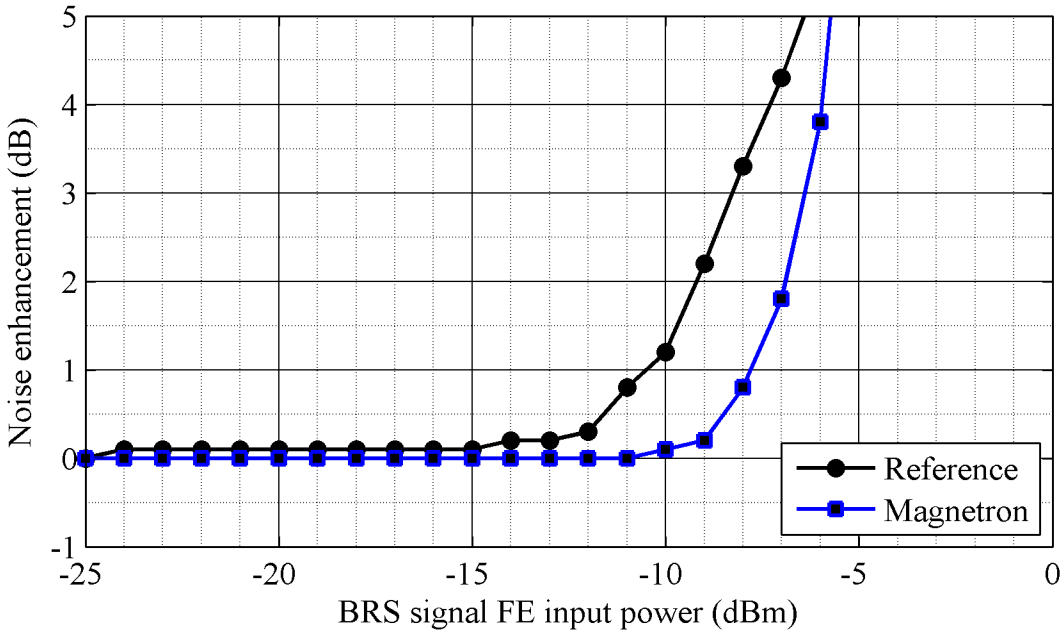

Figure 29. System noise enhancement.

7 CONCLUSION

This report describes a methodology for analyzing magnetron radar receiver front-end overload caused by signals from an aggregate of broadband radio service (BRS) base stations transmitting at frequencies within the radar front-end bandwidth.

The analysis in this report determines how much front-end filter attenuation is needed for various separation distances. The attenuation is the difference between the interfering power at the radar low-noise front-end (LNFE) and the allowable interference power.

The interfering power present at the LNFE is determined with a propagation model and a methodology for aggregating the signals from a network of base stations. Because of non-linear analytic complexity, allowable interference power, I_a, is determined by probability of detection laboratory measurements.

Two front-ends were examined. The first was an off-the-shelf magnetron radar front-end assembly with a circulator, limiter, and low-noise front-end. The second was what we refer to as a reference front-end consisting of a low-noise front-end constructed from discrete RF components. The reference front-end had approximately the same characteristics as the magnetron front-end assembly. However, the reference front-end did not have the filtering provided by the magnetron front-end assembly circulator and limiter.

The 5% degradation point (5% DP) measurements found I_a to be -11.5 and -9 dBm for the reference front-end and magnetron front-end assembly, respectively. Propagation analysis showed that interference powers were less than -23.6 dBm at a 1 km separation distance from the closest base station. Consequently, the front-end does not need filter attenuation for distances as close as 400 meters. Distances less than 400 meters were not analyzed due to antenna near field effects. Since the magnetron front-end assembly I_a is greater than the reference front-end's, this result would be true for the magnetron front-end assembly as well.

Gain compression and noise enhancement metrics, which are simpler to measure than the 5% DP metric, were also evaluated to determine if they could reliably predict I_a. We found that only the noise enhancement metric predicted it for both front-ends. This result is important since many front-end overload studies are based on the gain compression metrics.

The results in this report are encumbered with two caveats. First, the results are for an FDD BRS base station signal that occupies one 10 MHz BRS channel. Results need to be adjusted to accommodate more channels. Second, these results are based on magnetron radar signal processing. Additional analysis is needed to assess the impact to solid state radar receivers because their signal processing is very different from that in the magnetron radar receivers. The signal processing affects sensitivity and estimates of front-end attenuation need to take this into account.

8 REFERENCES

[1] International Telecommunication Union, "Procedures for determining the potential for interference between radars operating in the radiodetermination service and systems in other services," Recommendation ITU-R M.1461-1, July 2003.

[2] International Telecommunication Union, "Tests illustrating the compatibility between maritime radionavigation radars and emissions from radiolocation radars in the band 2900–3100 MHz," Report ITU-R M.2032, 2003.

[3] F. Sanders et. al., "Effects of RF interference on radar receivers," NTIA Report TR-06-444, September 2006. http://www.its.bldrdoc.gov/publications/2481.aspx

[4] J.E. Carroll, G.A. Sanders, F.H. Sanders, and R.L. Sole, "Case study: Investigation of interference into 5 GHz weather radars from unlicensed national information infrastructure devices, Part I," NTIA Technical Report TR-11-473, November 2010. http://www.its.bldrdoc.gov/publications/2548.aspx

[5] A. Paul et. al., "Interference protection criteria," NTIA Report 05-432, October 2005. http://www.its.bldrdoc.gov/publications/2462.aspx

[6] International Telecommunication Union, "Studies on frequency-related matters on International Mobile Telecommunications and other terrestrial mobile broadband applications", Resolution 233 (WRC-12),The World Radiocommunication Conference (Geneva, 2012)

[7] International Electrotechnical Commission (IEC), "Maritime navigation and radiocommunication equipment and systems – Shipborne radar – Performance requirements, methods of testing and required test results," IEC 62388, Edition 1.0, 2007-12.

[8] International Maritime Organization, "Adoption of the revised performance standards for radar equipment," Annex 34, Resolution MSC.192(79), December 6, 2004.

[9] Institute for Electrical and Electronic Engineers, "IEEE recommended practice for the analysis of in-band and adjacent band interference and coexistence between radio systems," IEEE Std 1900.2-2008, July 29, 2008.

[10] United Kingdom of Great Britain and Northern Ireland, "Radar adjacent band selectivity," Recommendation ITU-R 5b/389-E, November 18, 2009.

[11] U.S. Department of Commerce, National Telecommunications and Information Administration, "An assessment of the near-term viability of accommodating wireless broadband systems in the 1675–1710 MHz, 1755–1780 MHz, 3500–3650 MHz, and 4200–4220 MHz, 4380–-4400 MHz bands," http://www.ntia.doc.gov/files/ntia/publications/fasttrackevaluation_11152010.pdf, October 2010.

[12] European Telecommunications Standards Institute, "Technical Specification, Digital cellular telecommunications system (Phase 2+); Universal Mobile Telecommunications System (UMTS); LTE; E-UTRA,UTRA, and GSM/Edge; Multi-Standard Radio (MSR) Base Station (BS) radio transmission and reception," ETSI TS 137 104 version 11.2.1 Release 11, Oct. 2012.

[13] International Telecommunication Union Joint Task Group 4-5-6-7, Appendix 1 "Characteristics of terrestrial IMT-Advanced systems for frequency sharing/interference analyses" in Attachment 1, "Protection criteria, system characteristics, related materials on modelling considerations and sharing studies already performed or underway in ITU-R related to the terrestrial services" in Annex 2 "Compilation of material maintained by the Joint Task Group 4-5-6-7 working groups" of Report on the Fourth meeting of the Joint Task Group 4-5-6-7, Document 4-5-6-7/393-E, October 30, 2013.

[14] WiMAX Forum, "Mobile WiMAX – Part 1: A Technical Overview and Performance Evaluation," WiMAX Forum white paper, August 2006.

[15] R. Achatz, P. McKenna, R. Dalke, N. DeMinco, F. Sanders, and J. Carroll, "Effect of broadband radio service reallocation on 2900–3100 MHz band marine radars: Background," NTIA Report TR-15-513, April 2015. http://www.its.bldrdoc.gov/publications/2795.aspx

[16] U.S. Department of Transportation, Federal Aviation Administration, "Status report: Assessment of compatibility of planned Liqhtsquared ancillary terrestrial component transmissions in the 1526-1536 MHz band with certified aviation GPS receivers," Redacted Version Cleared for Public Release, January 25, 2012.

[17] R.J. Achatz, "Tutorial on using amplitude probability distributions to characterize the interference of ultrawideband transmitters to narrowband receivers," Appendix A in *The Temporal and Spectral Characteristics of Ultrawideband Signals*, NTIA Report 01-383, Jan. 2001. http://www.its.bldrdoc.gov/publications/2414.aspx

[18] M. Cotton, R. Achatz, J. Wepman, and B. Bedford, "Estimating and graphing the amplitude probability distribution of complex-baseband signals," Appendix D in "*Interference Potential of Ultrawideband Signals, Part 1: Procedures to characterize ultrawideband emissions and measure interference susceptibility of C-band satellite digital television receivers*", NTIA Report TR-05-419, Feb. 2005. http://www.its.bldrdoc.gov/publications/2449.aspx

[19] R.G. Meyer and A. K. Wong, "Blocking and desensitization in RF amplifiers," *IEEE Journal of Solid-State Circuits*, Vol. 30, No. 8, August 1995, pp. 944-946.

[20] N. Garmendia and J. Protilla, "Study of PM noise and noise figure in low noise amplifiers working under small and large signal conditions," *IEEE/MTT-S International Microwave Symposium*, 2007.

[21] G.A. Hufford, A.G. Longley, and W.A. Kissick, “A Guide to the use of the ITS irregular terrain model in the area prediction mode,” NTIA Report 82-100, April 1982. http://www.its.bldrdoc.gov/publications/2091.aspx

[22] N. DeMinco, “Propagation loss prediction considerations for close-in distances and low-antenna height applications,” NTIA Report TR-07-449, July 2007. http://www.its.bldrdoc.gov/publications/2486.aspx

9 ACKNOWLEDGEMENTS

This work was sponsored by the U.S. Coast Guard Spectrum Management Telecommunications Policy Division, U.S. Coast Guard CG-652, 2100 2nd St. SW Stop 7101, Washington DC 20593-7101. The authors would like to acknowledge Fred Mistichelli (former Division Chief), Joseph Hersey (former Division Chief), and Daniel Freedman (former Spectrum Engineer) for their sponsorship.

The authors would also like to acknowledge David Turnage, Research and Development Manager, Kelvin Hughes Ltd., for sharing his insights into this issue.

Finally, the authors would also like to acknowledge Al Romero, Visual Information Specialist, at the National Oceanic and Atmospheric Administration (NOAA) for creating the illustrative figures, Brent Bedford (ITS) for consultations on test fixture instrumentation, Wayde Allen (ITS) for consultations on electromagnetic shielding, and Iris Tobias (ITS) for equipment construction.

APPENDIX A: EFFECT OF INTERFERENCE ON APD AND PSD

In this Appendix, reference and magnetron front-end amplitude probability distributions and power spectral densities for the Swerling 0 case (without target radar cross section fluctuation) with no integration are shown at three interference power levels corresponding to levels where interference 1) had no measurable effect on P_d = 0.8, 2) caused P_d to degrade to 0.75 or less, and 3) caused P_d to degrade to 0.5 or less. The SNR to achieve P_d = 0.8 with a P_{fa} = 10^{-4} for Swerling 0 with no integration is 10.98 dB.

The data for the APDs and PSDs in Figures A-1-A-12 was collected with a 5.9375 MHz sample rate corresponding to a 4.6386 MHz VSA span. Noise and signal APDs at a bandwidth corresponding to the VSA span are constructed from 3,072,000 and 307,200 samples, respectively. Only one in three of the samples were used in the APD to assure independence.

Noise and signal complex baseband PSDs are estimated with the Welch method by averaging the amplitude of 128 spectrum created from 1024 sample block sizes. A Hamming window with a 1.36 frequency bin equivalent noise bandwidth was used to limit spectral leakage. The corresponding frequency bin and equivalent noise bandwidth are 5798 and 7885 Hz, respectively. The spike at the 0 Hz center frequency in the signal plus noise PSDs is the desired signal. The magnetron front-end assembly PSDs have three discrete spikes on either side of the center frequency. The amplitude and frequency of the spikes do not change with interference power level.

The results in Table A-1 show that degradation in the reference front-end is due to a combination of gain compression, i.e. decreasing S, and noise enhancement, i.e. increasing V_T. The noise APDs show a definite increase in impulsiveness corresponding to increased interference power at percentiles exceeding 0.01%. This effect is more pronounced in the magnetron front-end. Changes in the PSD are not evident.

Table A-1. Power levels and probability of detection for reference front-end and magnetron front-end assembly.

Front-end	I **(dBm)**	S **(dBm)**	N **(dBm)**	S/N **(dB)**	V_T **(dBm)**	P_d
Reference	-25	-38.7	-49.7	11.0	-40.8	0.7979
Reference	-15	-39.0	-49.8	10.7	-40.1	0.7366
Reference	-12	-39.6	-49.5	10.0	-39.5	0.5177
Magnetron	-25	-38.1	-49.2	11.1	-39.5	0.8155
Magnetron	-10	-38.3	-48.9	10.7	-39.1	0.7119
Magnetron	-9	-38.3	-48.7	10.4	-36.9	0.2375

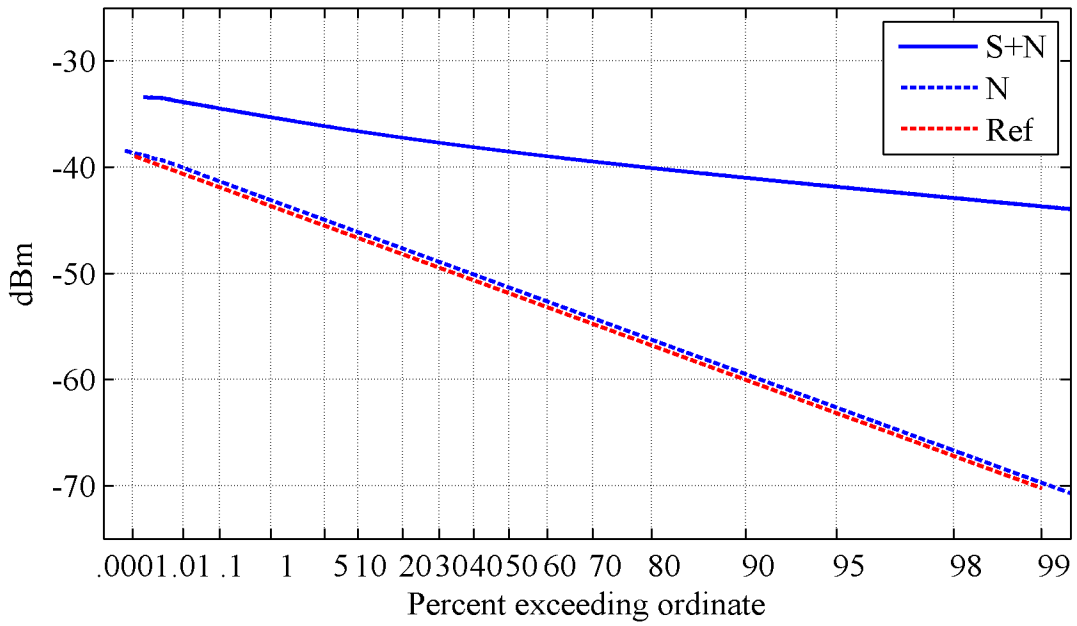

Figure A-1. Reference front-end APD at I = -25 dBm.

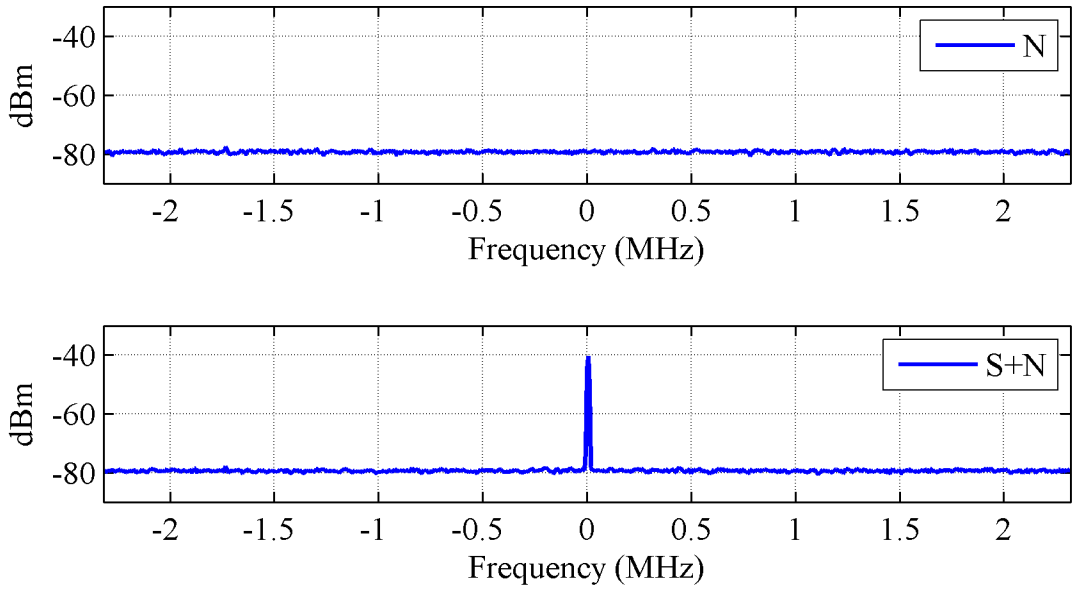

Figure A-2. Reference front-end PSD at I = -25 dBm.

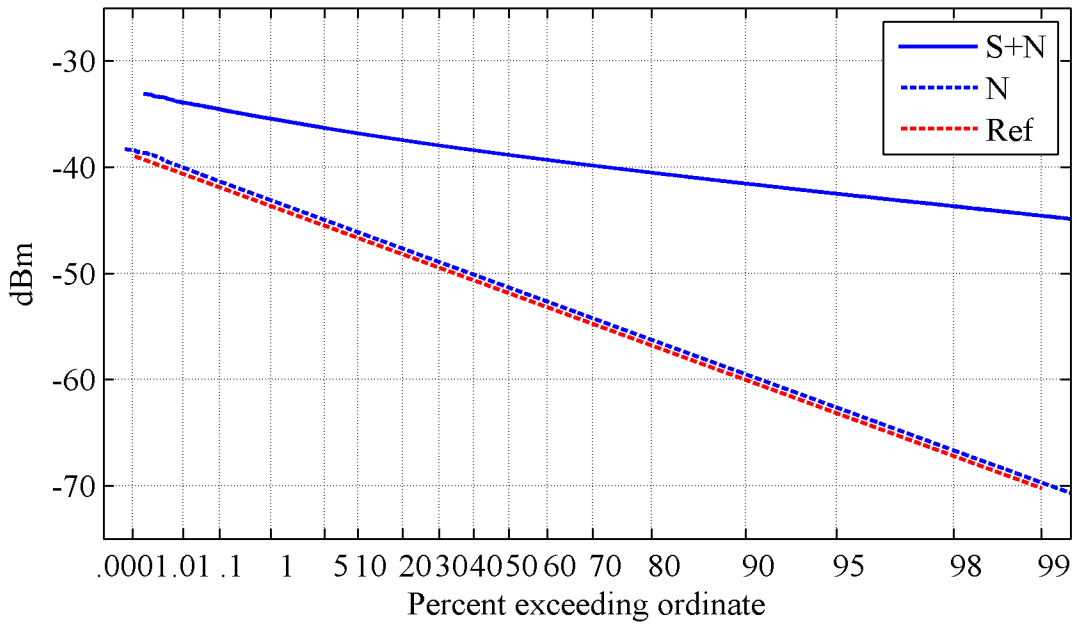

Figure A-3. Reference front-end APD at I = -15 dBm.

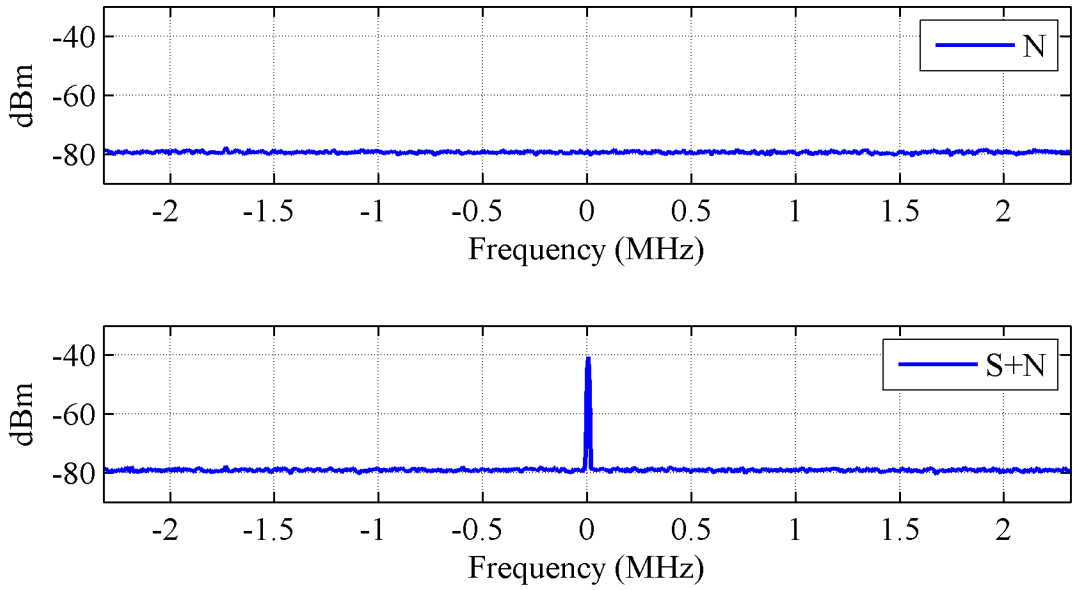

Figure A-4. Reference front-end PSD at I = -15 dBm.

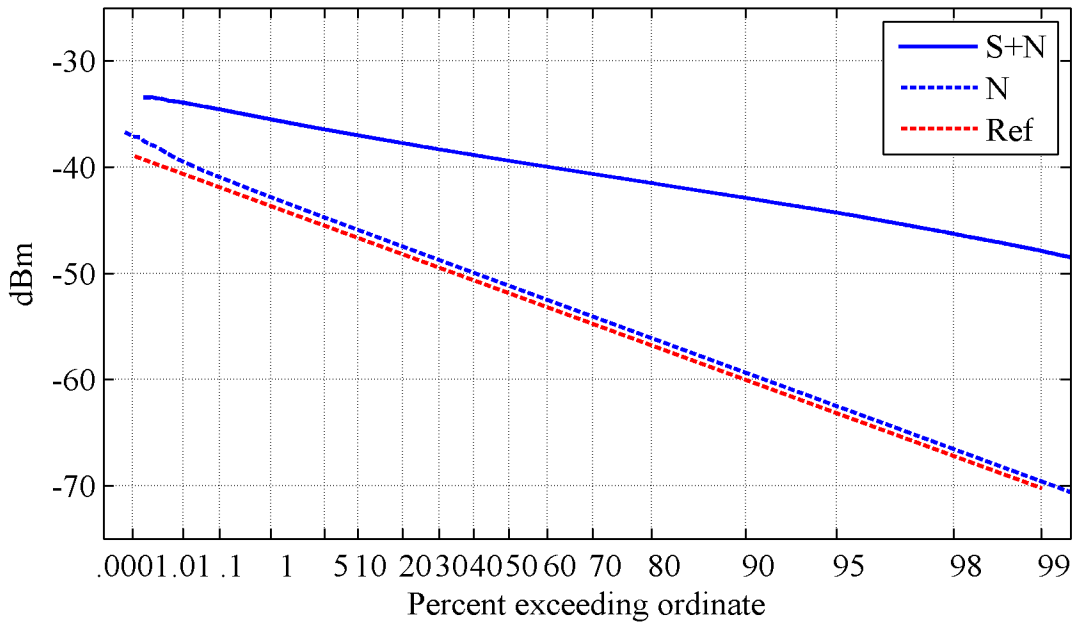

Figure A-5. Reference front-end APD at I = -12 dBm.

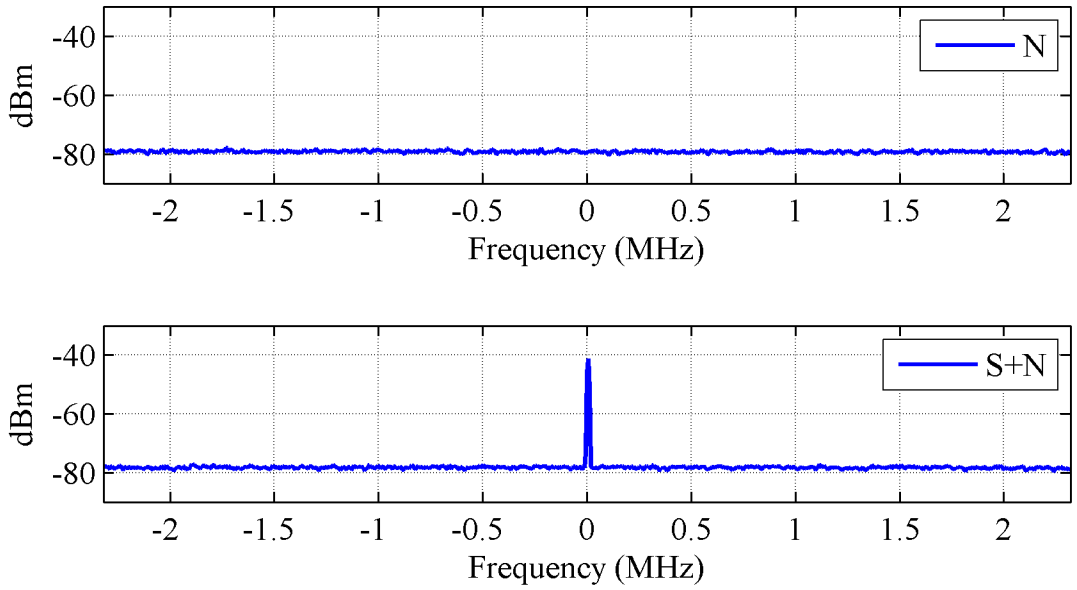

Figure A-6. Reference front-end PSD at I = -12 dBm.

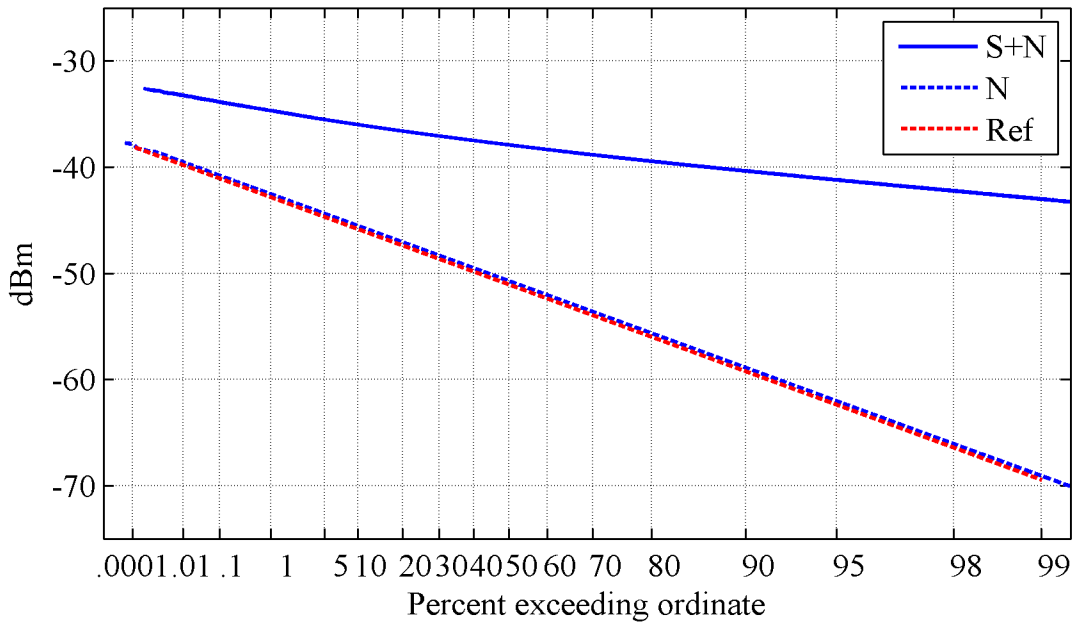

Figure A-7. Magnetron front-end assembly APD at *I* = -25 dBm.

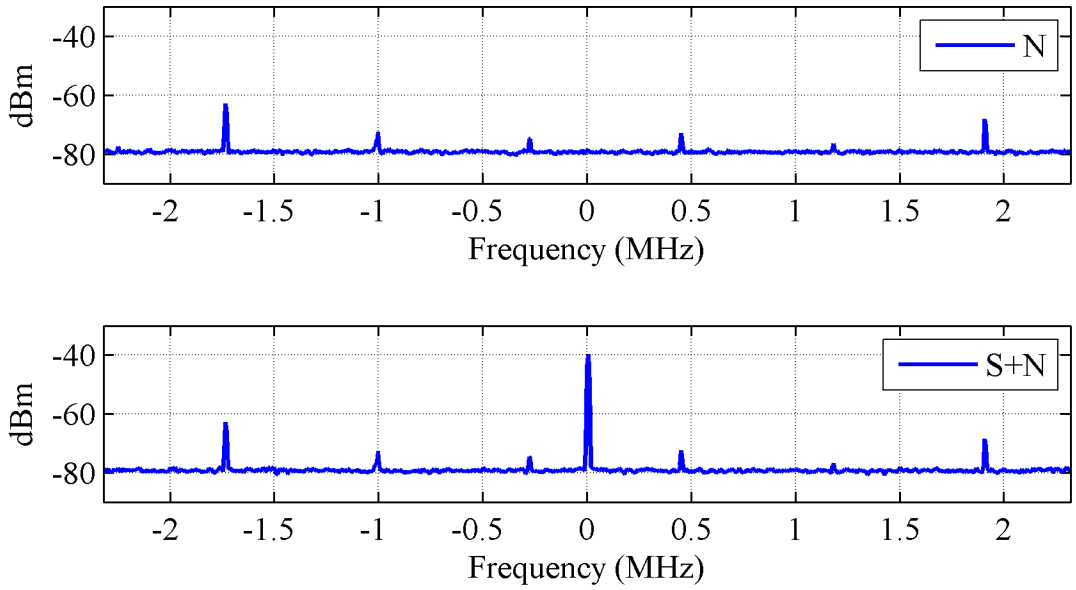

Figure A-8. Magnetron front-end assembly PSD at *I* = -25 dBm.

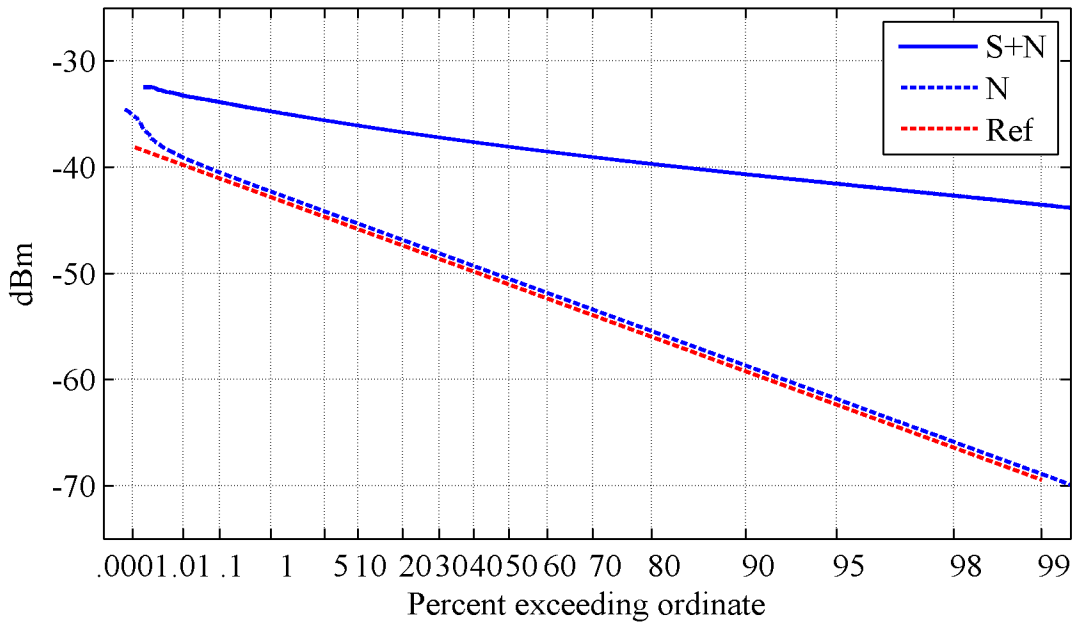

Figure A-9. Magnetron front-end assembly APD at I = -10 dBm.

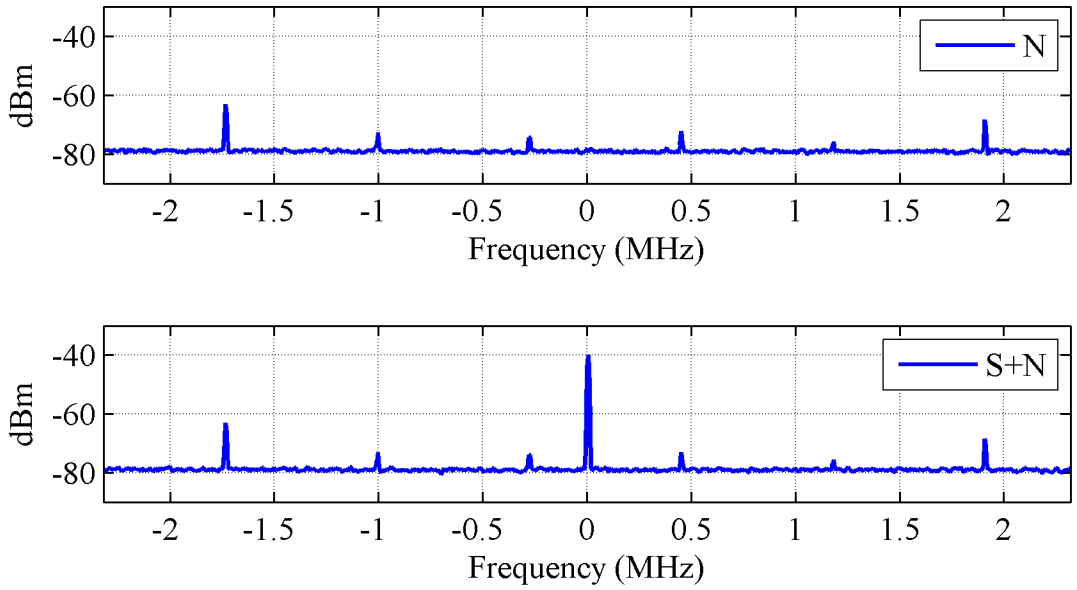

Figure A-10. Magnetron front-end assembly PSD at I = -10 dBm.

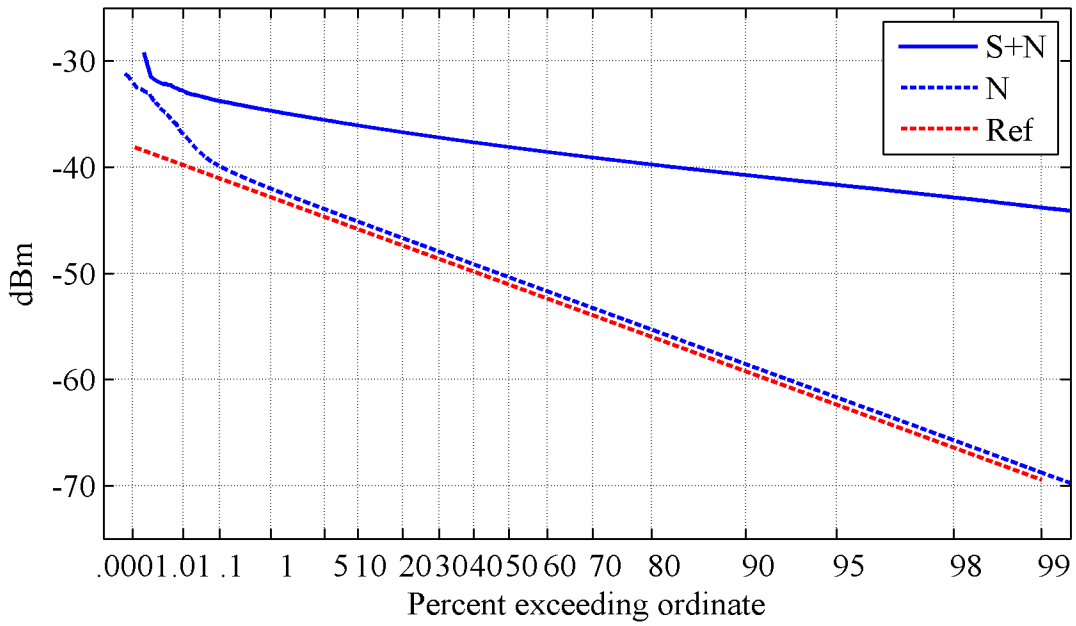

Figure A-11. Magnetron front-end assembly APD at *I* = -9 dBm.

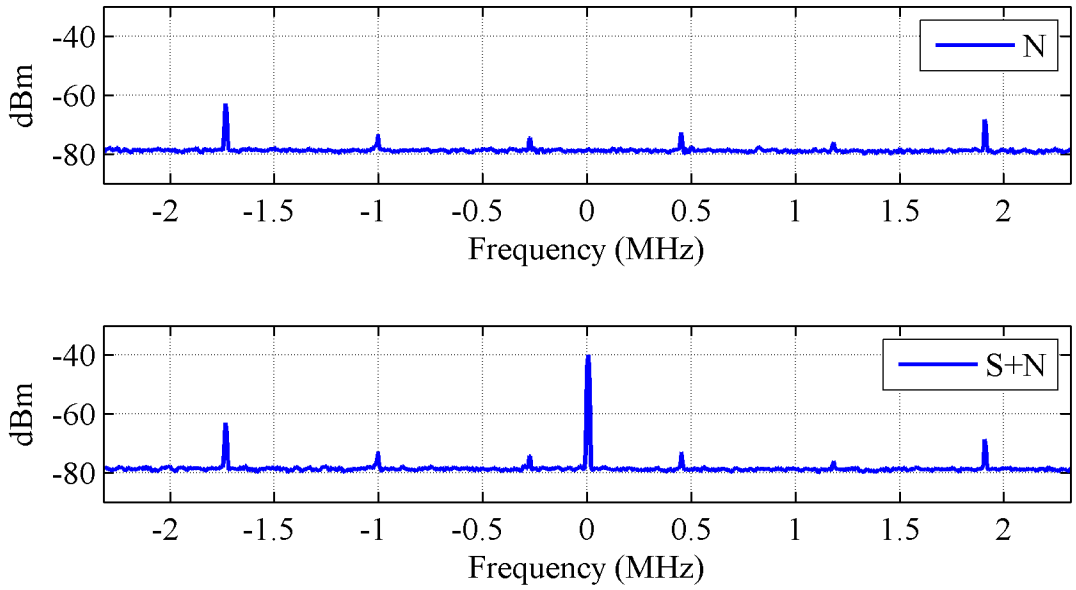

Figure A-12. Magnetron front-end assembly PSD at *I* = -9 dBm.

APPENDIX B: UNCERTAINTY

Measurement uncertainty considerations determined the number of APD points and target RCS fluctuations. This Appendix describes how we calculated these numbers.

Each measurement begins by obtaining the voltage threshold quantile, V_T, corresponding to the probability of false alarm, p_{fa}, from a measured noise APD

$$V_T = V[\kappa] \tag{B-1}$$

where

$$\kappa = \lfloor N p_{fa} \rfloor \tag{B-2}$$

$\lfloor \cdot \rfloor$ is the integer floor operator, and N is the number of APD samples.

The true probability corresponding to V_T is

$$p = Pr\{V > V_T\} \tag{B-3}$$

whereas the estimated probability is

$$\hat{p} = \frac{\kappa}{N}$$

We want to find N and an interval $[p_-, p_+]$ so that

$$Pr\{p_- < p < p_+\} = c \tag{B-4}$$

i.e. $[p_-, p_+]$ is the $c \cdot 100$ % confidence interval.

We begin with the known probability distribution of the estimate $\hat{p}$ and set [B-1],[B-2]

$$Pr\{\hat{p}_- < \hat{p} < \hat{p}_+\} = c \tag{B-5}$$

where

$$\hat{p}_- = p - z\sqrt{pq/N} \tag{B-6}$$

$$\hat{p}_+ = p + z\sqrt{pq/N} \tag{B-7}$$

$$q = 1 - p \tag{B-8}$$

z is the number of standard deviations and the standard deviation of $\hat{p}$ is

$$\sqrt{pq/N}. \tag{B-9}$$

The number of standard deviations and confidence are related by

$$\Phi(z) = \frac{1}{\sqrt{2\pi}} \int_{-\infty}^{z} e^{-t^2/2} dt = \frac{1+c}{2} \tag{B-10}$$

$$\mathrm{z} = \Phi^{-1}\left(\frac{1+c}{2}\right) \tag{B-11}$$

Simplifying (B-6) and (B-7) to

$$\hat{p} = p \pm z\sqrt{pq/N} \tag{B-12}$$

subtracting p from both sides, squaring, and rearranging into quadratic terms with respect to p

$$\left(\frac{N}{N+z^2}\right)p^2 - \left(2\hat{p} + \frac{z^2}{2N}\right)p + \hat{p}^2 = 0 \tag{B-13}$$

solving with the quadratic formula, and factoring we arrive at [B-3]

$$p = \left(\frac{N}{N+z^2}\right)\left(\hat{p} \pm z\sqrt{\frac{\hat{p}\hat{q}}{N} + \frac{z^2}{4N^2}} + \frac{z^2}{2N}\right) \tag{B-14}$$

Expanding the first term into a Taylor series yields

$$\frac{N}{N+z^2} = \frac{1}{1+\frac{z^2}{N}} = 1 - \frac{z^2}{N}\cdots = 1 - O\left(\frac{1}{N}\right) \tag{B-15}$$

where $O(\cdot)$ is the order operator characterizing extinction rate. Factoring and expanding one of the square root terms into a Taylor series

$$z\sqrt{\frac{\hat{p}\hat{q}}{N} + \frac{z^2}{4N^2}} = z\sqrt{\frac{\hat{p}\hat{q}}{N}}\sqrt{1 + \frac{z^2}{4\hat{p}\hat{q}N}} = z\sqrt{\frac{\hat{p}\hat{q}}{N}}\left(1 - O\left(\frac{1}{N}\right)\right) \tag{B-16}$$

we have

$$p = \left(1 - O\left(\frac{1}{N}\right)\right)\left(\hat{p} + z\sqrt{\frac{\hat{p}\hat{q}}{N}}\left(1 - O\left(\frac{1}{N}\right)\right) + \frac{z^2}{2N}\right) \tag{B-17}$$

For large $N \gg z$ the approximate lower and upper bounds for the $c \cdot 100$ % confidence interval are

$$p_{-} = \hat{p} - \sqrt{\hat{p}\hat{q}/N}\,\Phi^{-1}\left(\frac{1+c}{2}\right) \tag{B-18}$$

and

$$p_+ = \hat{p} + \sqrt{\hat{p}\hat{q}/N}\,\Phi^{-1}\left(\frac{1+c}{2}\right) \tag{B-19}$$

The corresponding lower and upper and bounds for the amplitude rank order indexes are

$$k_- = \left[N\hat{p} - \sqrt{N\hat{p}\hat{q}}\Phi^{-1}\left(\frac{1+c}{2}\right)\right] \tag{B-20}$$

and

$$k_+ = \left[N\hat{p} + \sqrt{N\hat{p}\hat{q}}\Phi^{-1}\left(\frac{1+c}{2}\right)\right] \tag{B-21}$$

Figures B-1 and B-2 show how the confidence interval changes when N is 10^6 and P_{fa} is 10^{-4}. At 68% confidence, $[p_-, p_+]$ = [0.00009, 0.00011], $[k_-, k_+]$ = [90, 110], and the fractional error is approximately 10%. The number of points can be decreased by an order of magnitude when measuring P_d which is of little concern below 10^{-3}.

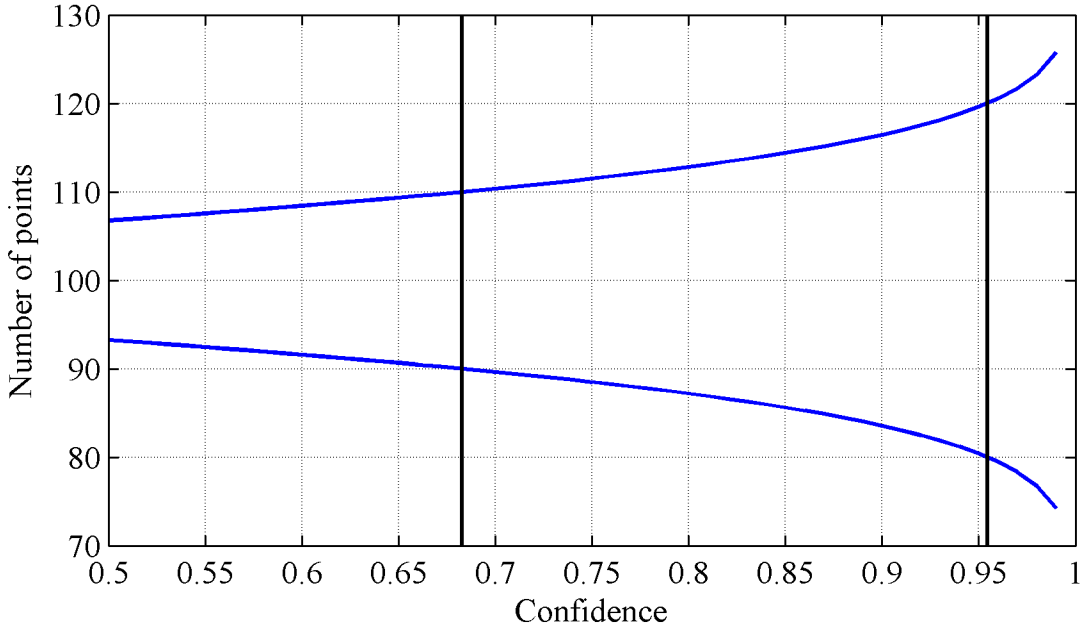

Figure B-1. APD uncertainty in number of points when 10^6 points are used with a 10^{-4} event probability. Vertical lines at 68.3 and 95.5 percent represent one and two standard deviations respectively.

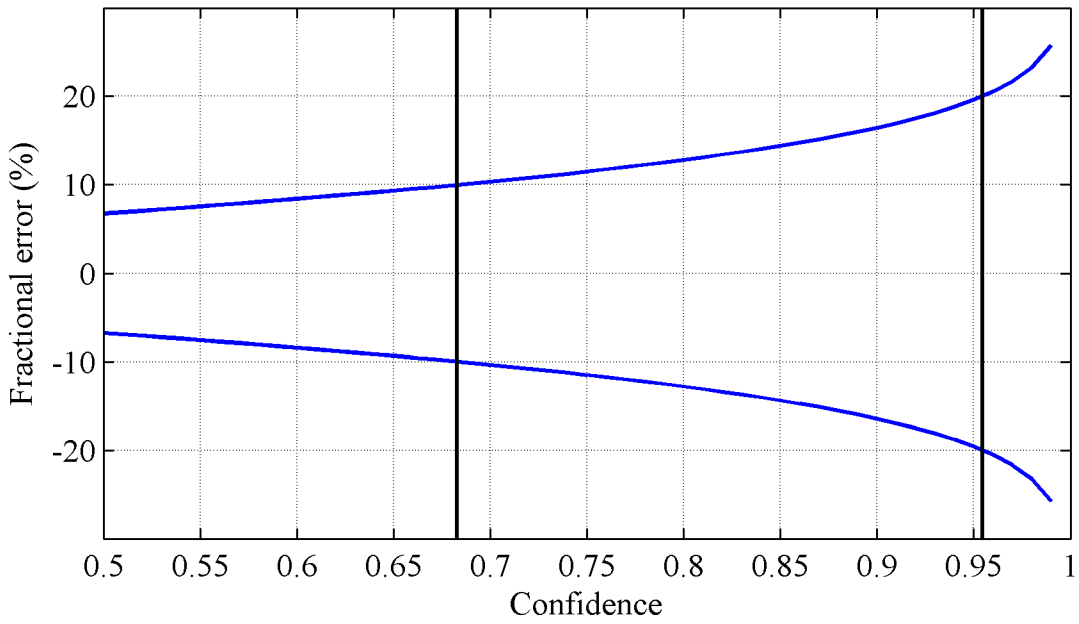

Figure B-2. APD uncertainty in fractional uncertainty when 10^6 points are used with a 10^{-4} event probability. Vertical lines at 68.3 and 95.5 percent represent one and two standard deviations respectively.

The number of target RCS fluctuations is determined from the uncertainty in the mean power. This uncertainty is evaluated by the standard deviation of the mean

$$\sigma_M = \frac{\sigma}{\sqrt{N}} \tag{B-22}$$

where σ is the standard deviation of the underlying Swerling 1 process. Figure B-3 shows how σ_M decreases with the number of fluctuations. Approximately 400 fluctuations are needed to reduce σ_M from 1 to 0.05 which corresponds to a 5% error or a 0.44 dB mean power deviation.

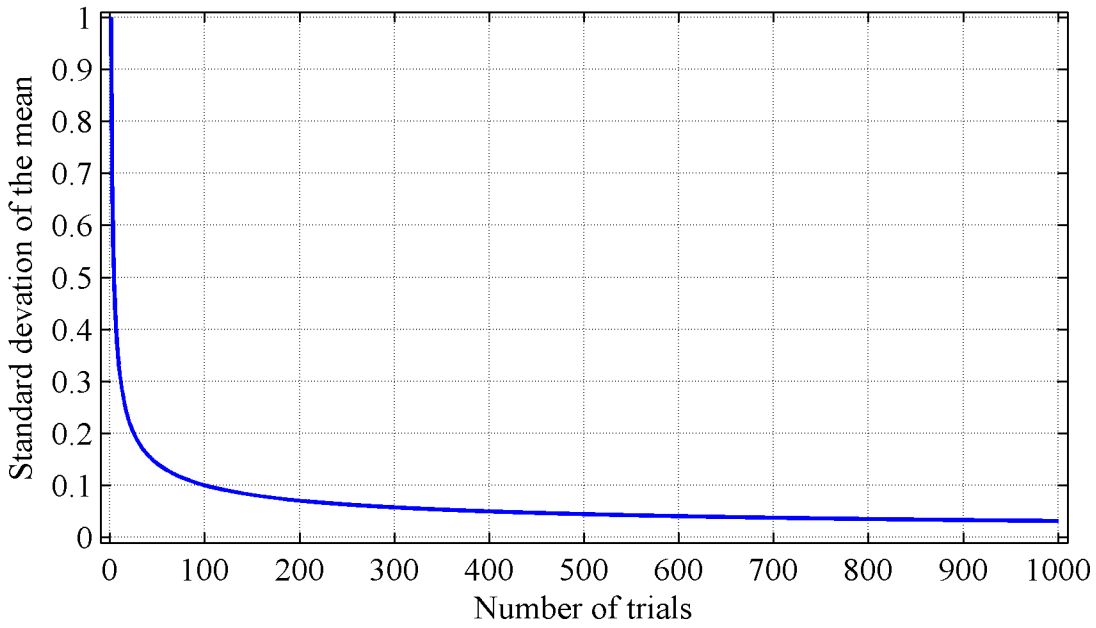

Figure B-3. Standard deviation of the mean power estimate as a function of the number of Swerling fluctuations.

A Monte Carlo simulation for Swerling 1 target RCS fluctuation with six integrations was performed to verify test fixture performance with these parameters. Figures B-4 and B-5 show the results of this simulation. The simulation was done without interference and non-linear effects. One million APD points were used to determine P_{fa} and one hundred thousand points were used to determine P_d. A 10.03 dB theoretical SNR is needed to achieve 0.8 and 10^{-4} for P_d and P_{fa}, respectively. The estimated P_d and SNR at the end of 1000 trials are 0.79 and 10.1 dB, respectively.

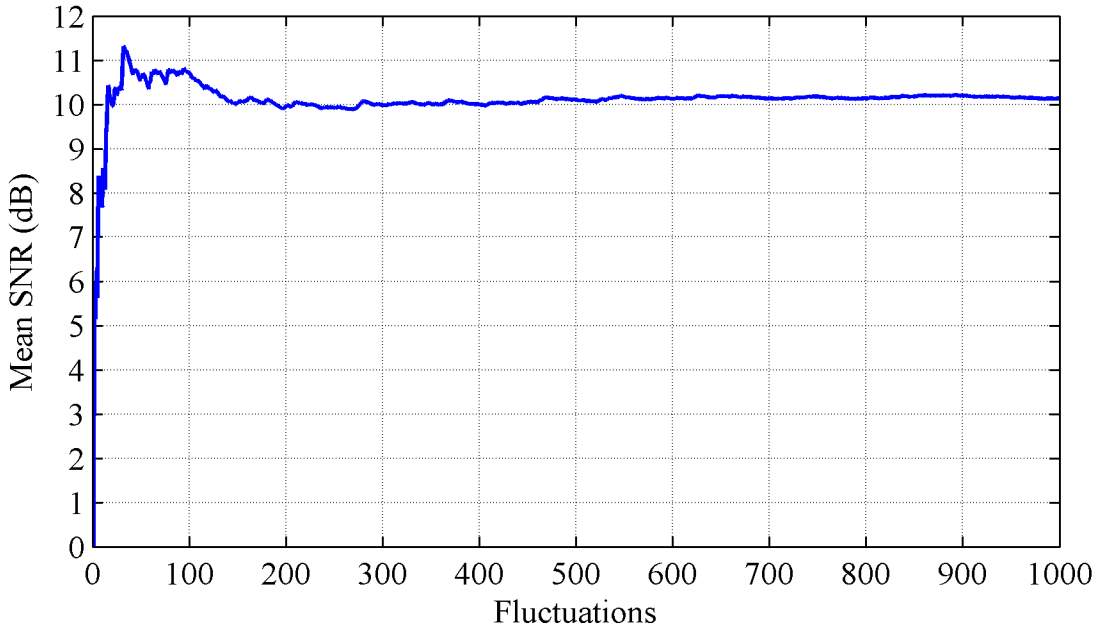

Figure B-4. Monte Carlo mean SNR results.

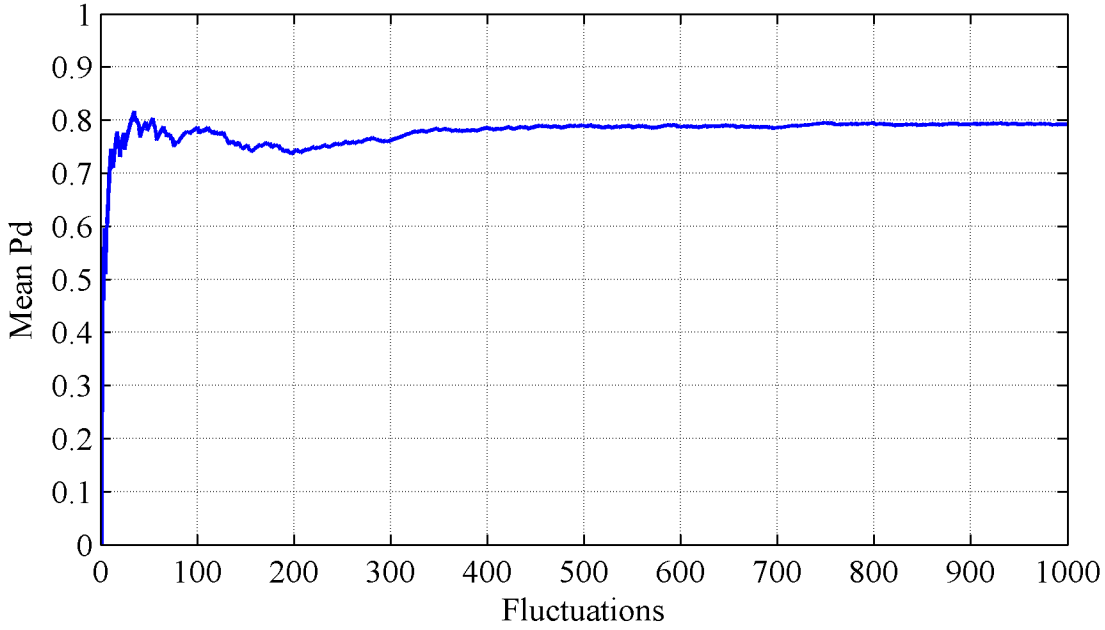

Figure B-5. Monte Carlo mean P_d results.

B.1 References

[B-1] R. Dalke, "Statistical Considerations for Noise and Interference Measurements," NTIA Technical Report TR-09-458, November 2008. http://www.its.bldrdoc.gov/publications/2495.aspx

[B-2] J. Walsh, *Handbook of Nonparametric Statistics*, Princeton, N.J., D. Van Nostrand Company, Inc., 1962, p. 193.

[B-3] H. Cramer, *Mathematical Methods of Statistics*, Princeton, N. J., Princeton University Press, 1954, p. 515.

APPENDIX C: SCHEMATICS AND SPECIFICATIONS

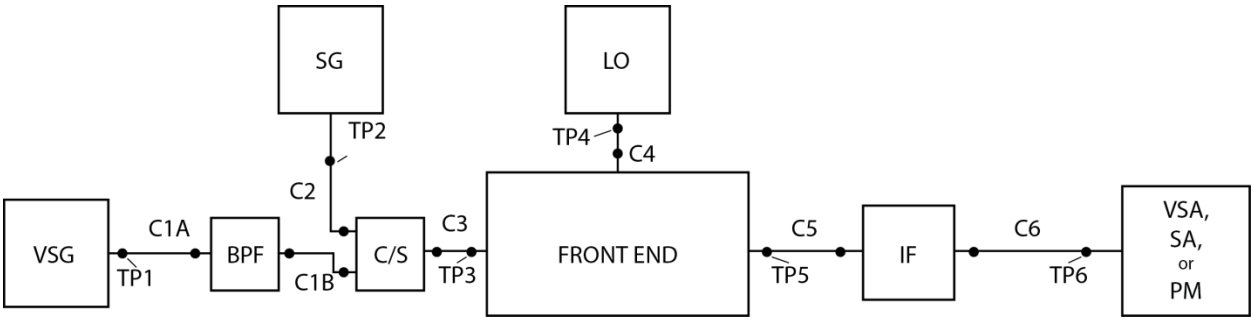

Figure C-1. Front-end overload test fixture with component, cable (Cx), and test point (TPx) identifiers. VSG represents the vector signal generator, BPF represents the band-pass filter, SG represents the signal generator, C/S represents the combiner/splitter, LO represents the local oscillator, VSA represents the vector signal analyzer, SA represents the spectrum analyzer, and PM represents the power meter.

Table C-1. Front-end overload test fixture components.

Identifier	Name	Model number	Notes
VSG	Vector signal generator	Agilent E4438c	S/N SG45090178
SG	Signal generator	Hewlett Packard 8648c	
LO	Signal generator	Hewlett Packard 8341b	
BPF	Tunable bandpass filter	Texscan 5VF 2000/4000	
C/S	Combiner/Splitter	Mini-Circuits ZAPD-4-S+	
VSA	Vector signal analyzer	Agilent 89600S	S/N US43490919
SA	Spectrum analyzer	Hewlett Packard 8562A	
PM	Power meter	Agilent E4417A	
IF	Intermediate Frequency section	Built at ITS	
	Rubidium clock	Lucent RFTGm-11-Rb	Connected to SG, LO, VSA, VSG, and SA

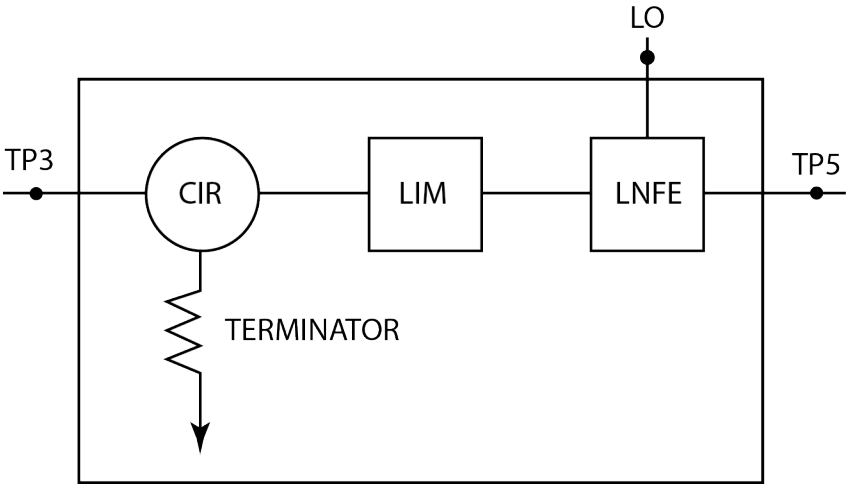

Figure C-2. Magnetron front-end assembly with test points (TP). CIR represents the circulator, LIM represents the limiter, and LNFE represents the low-noise front-end.

Table C-2. Magnetron front-end assembly components.

Identifier	**Name**	**Model number**	**Notes**
CIR	Circulator	New Japan Radio NJC3311A	Waveguide
TERM	Waveguide WR284 to N adaptor terminated with 50ohm load	Advanced Technical Materials PNR 284-253A	
LIM	Limiter	New Japan Radio NJS6318	Waveguide
LNFE	Low-noise front-end	New Japan Radio NJS4310D	

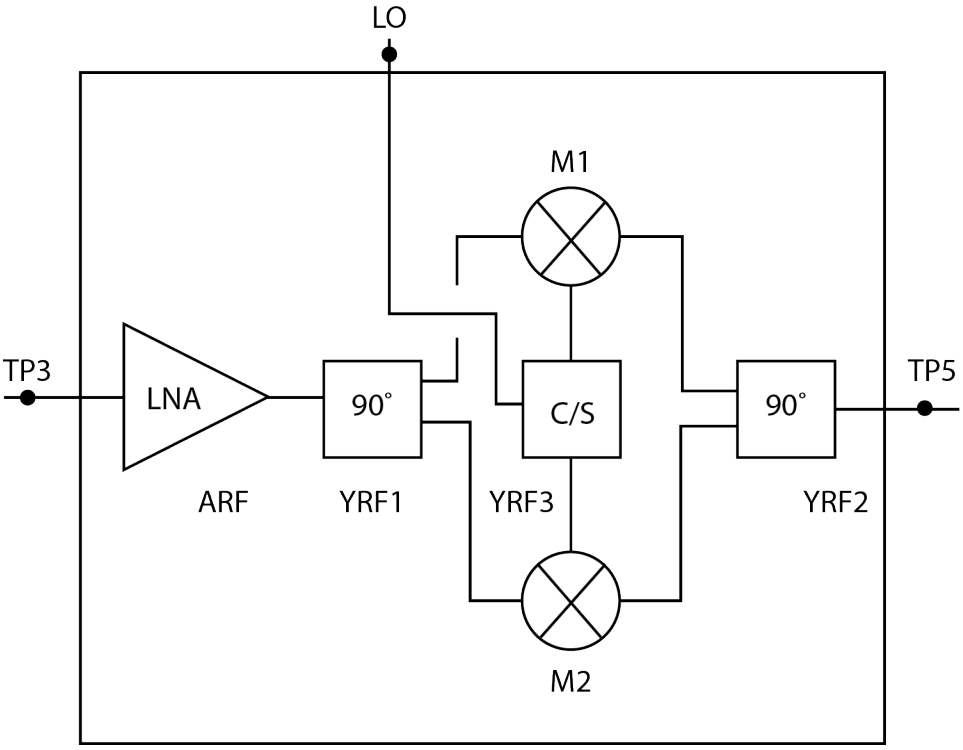

Figure C-3. Reference front-end with test points (TP). LNA represents the low-noise amplifier, 90^{o} represents the quadrature combiner/splitter, C/S represents the combiner/splitter, and circles with a cross represent a mixer. The mixing stage is implemented with two mixers, M1 and M2, to attenuate noise at image frequency.

Table C-3. Reference front-end components.

Identifier	**Name**	**Model number**	**Notes**
ARF	Low-noise Amplifier	Mini Circuits ZX-606013E-S+	
YRF1	90^{0} Combiner/Splitter	Mini Circuits ZAPDQ-4-S	
YRF2	Combiner/Splitter	Mini Circuits ZMSCQ-2-90	
YRF3	90^{0} Combiner/Splitter	Mini Circuits ZAPD-4-S+	
M1 and M2	Mixer	Mini Circuits ZX-05C42CH-S+	

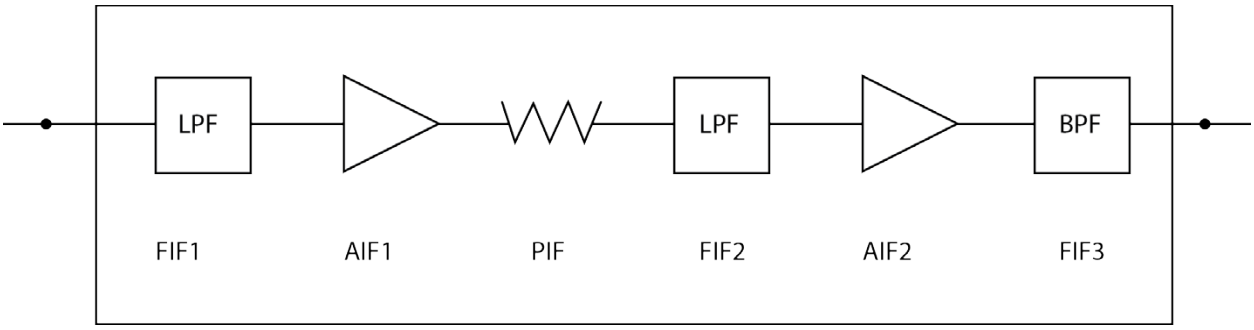

Figure C-4. IF section. LPF represents the low pass filter and BPF represents the BPF.

Table C-4. IF section components.

Identifier	**Name**	**Model number**	**Notes**
FIF1, FIF2	Low pass filter	Mini-Circuits SLP-100+	100 MHz bandwidth
AIF1, AIF2	Amplifier	Mini-Circuits ZFL-500+	
PIF	Attenuator		
FIF3	Band pass filter	Mini-Circuits SBP-60+	20 MHz bandwidth

APPENDIX D: POWER MEASUREMENT AND CALIBRATION

D.1 Sine Wave Power Measurement

- The spectrum (SA) or vector signal analyzer (VSA) is used to measure sine wave power so that the bandwidth can be restricted and noise eliminated as much as possible from the measurement. The sine wave should be well above (30 dB) the noise floor. Auto-couple span, sweep time, and video bandwidth. Peak and RMS detector should give same result for sine measurement. Measure with peak search function.

D.2 Noise Power Measurement

- The power meter (PM) is used to do noise measurements.
- SA or VSA can also be used to do average noise power measurements. RMS voltage detection is the preferred method.
- If using an SA without RMS voltage detection, the measurement can be made with analog or digital video averaging. However, the displayed value will be lower than the actual value and must be corrected

$$P_{av} = P_{SA} + 1.05 + 1.45\ (dB) - 0.5\ (dB) \quad \text{(D-1)}$$

where 1.05 dB compensates for envelope detection, the 1.45 dB compensates for the log amplification, and the -0.5 dB converts the Gaussian filter 3 dB bandwidth to an equivalent noise bandwidth.

D.3 Signal Generator Power Verification

1. Make sure the signal generator (SG), vector signal generator (VSG), VSA, SA, and PM have up to date certifications.
2. Calibrate VSG using I/Q>User Cal>Set Range
3. Set VSG or SG to generate a -30 dBm sine wave.
4. Measure power with PM.
5. Note any deviation.

APPENDIX E: CHARACTERIZATION PROCEDURES

This section describes gain and noise figure characterizations for the front-end (FE) and intermediate frequency (IF) sections. The FE and IF combined is referred to as the system.

E.1 IF Gain and Gain Compression

1. Estimate IF gain, G_{if}, from component specifications.
2. Estimate output 1 dB compression point from component specifications.
3. Estimate the input 1 dB compression point.

$$P_{in,1dB} = P_{out,1dB} - G_{if} \ (dB) \tag{E-1}$$

4. Measure cable loss of input, L_1, and output, L_2, cables at the IF frequency.
5. Set signal generator (SG) to generate sine wave.
6. Set SG to IF frequency.
7. Set SG to a power, P_{SG}, that will generate a power at the spectrum analyzer, P_{SA}, well above spectrum analyzer noise floor. Check to make sure it will not overload last IF amplification stage.
8. Set up equipment as shown in Figure E-(a).
9. Measure power, P'_{SA}, without IF section.

$$P'_{SA} = P_{SG} - L_1 - L_2 \ (dB) \tag{E-2}$$

10. Set up equipment as shown in Figure E-(b).
11. Measure power, P_{SA}, with IF section.
12. Calculate input power, P_1, and output power, P_2.

$$P_1 = P_{SG} - L_1 \ (dB) \tag{E-3}$$

$$P_2 = P_{SA} + L_2 \ (dB) \tag{E-4}$$

13. Calculate IF gain

$$G_{if} = P_2 - P_1 \ (dB) \tag{E-5}$$

$$G_{if} = P_{SA} - P'_{SA} \ (dB) \tag{E-6}$$

14. Set P_{SG} so that P_1 is 20 dB below estimated 1dB compression point.

$$P_{SG} = P_1 + L_1\ (dB) \quad \text{(E-7)}$$

15. Measure P_{SA} and calculate P_2.

$$P_2 = P_{SA} + L_2\ (dB) \quad \text{(E-8)}$$

16. Repeat, increasing P_{SG} in 1 dB steps, until P_{SA} does not change.

17. Plot input power, P_1, versus output power, P_2.

E.2 FE Gain and Gain Compression

1. Estimate FE gain from component specifications.
2. Estimate output 1 dB compression point from component specifications.
3. Estimate the input 1 dB compression point.
4. Set SG to generate sine wave.
5. Set SG to RF frequency.
6. Set SG to a power, P_{SG}, that will generate a power at the spectrum analyzer, P_{SA}, well above spectrum analyzer noise floor. Check to make sure it will not overload the FE.
7. Measure cable loss L_1 at the RF frequency.
8. Measure cable loss L_2 at the IF frequency.
9. Set up equipment as show in Figure E-(c).
10. Measure P_{SA}.
11. Calculate RF gain.

$$G_{fe} = P_2 - P_1(dB) \quad \text{(E-9)}$$

$$G_{fe} = P_{SA} - P_{SG} + L_2 + L_1\ (dB) \quad \text{(E-10)}$$

12. Set P_{SG} so that P_1 is 20 dB below estimated 1dB compression point.

$$P_{SG} = P_1 + L_1\ (dB) \quad \text{(E-11)}$$

13. Measure P_{SA} and calculate P_2.

$$P_2 = P_{SA} + L_2\ (dB) \quad \text{(E-12)}$$

14. Repeat by increasing P_{SG} in 1 dB steps until P_{SA} does not change.

15. Plot input power, P_1, versus output power, P_2.

E.3 System Gain and Gain Compression

1. Set up equipment as shown in Figure E-1(d).

2. Measure system gain, G_{sys}, and gain compression the same as was done for the FE.

3. Compare to G_{sys} calculated from

$$G_{sys} = G_{if} + G_{fe} - L_3 \ (dB) \tag{E-13}$$

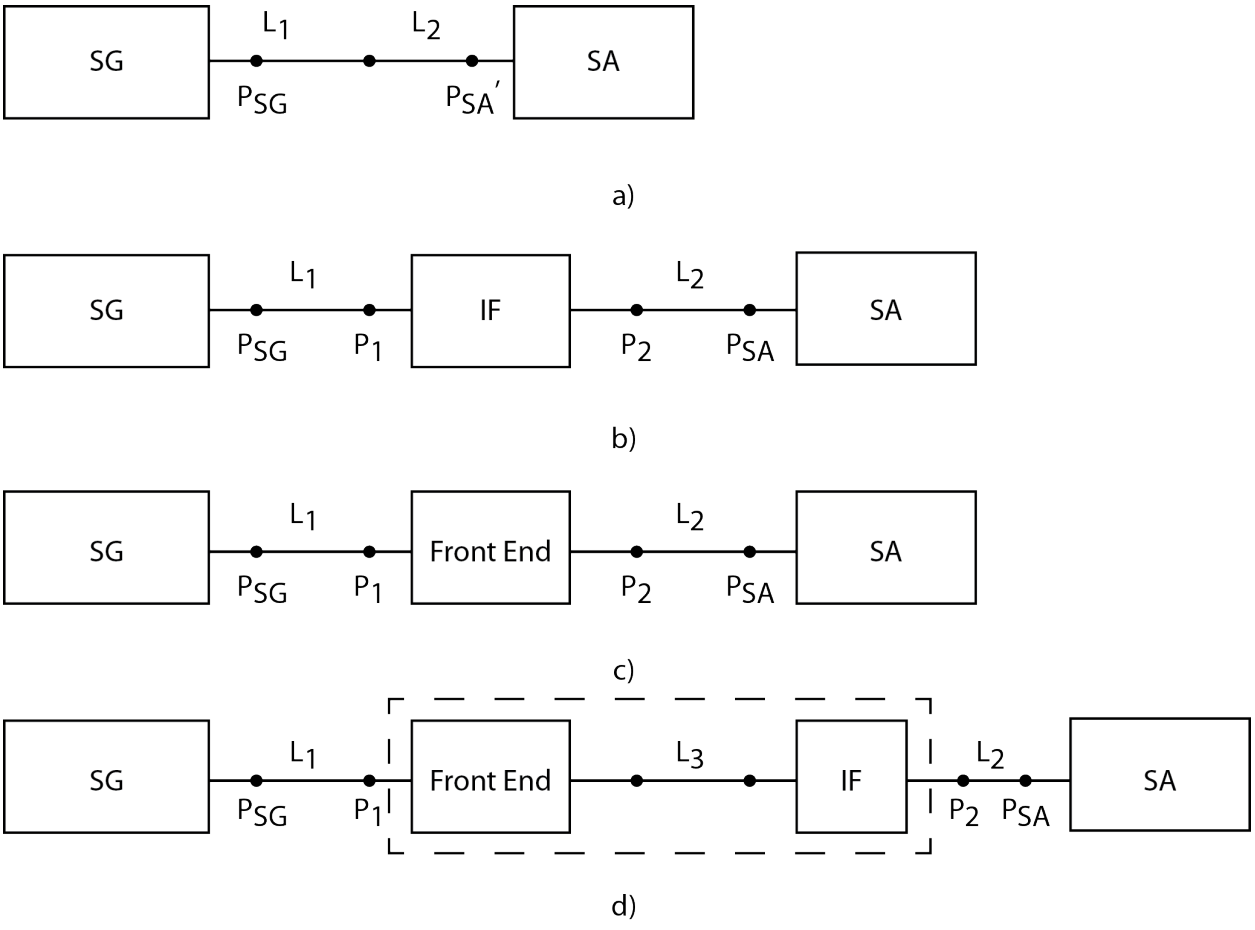

Figure E-1. Gain measurement configurations. SG represents the signal generator and SA represents the spectrum analyzer.

E.4 IF Noise Figure

1. Set up equipment as shown in Figure E-2(a).

2. Turn noise diode (ND) off and measure power at IF output, P_{OFF}.

3. Turn ND on and measure power at IF output, P_{ON}.

4. Calculate noise figure

$$F_{if} = ENR - 10\log_{10}\left(\frac{P_{ON}}{P_{OFF}} - 1\right)\ (dB) \tag{E-14}$$

where ENR is the noise diode excess noise ratio in dB.

E.5 System and FE Noise Figure

1. Set up equipment as shown in Figure E-2(b).

2. Connect IF section.

3. Measure system noise figure, F_{sys}, using ND as is done for IF.

4. Calculate the noise figure of the FE alone by

$$f_{fe} = f_{sys} - \frac{f_{if} - 1}{g_{fe}} \tag{E-15}$$

$$F_{fe} = 10\log_{10}(f_{fe})\ (dB) \tag{E-16}$$

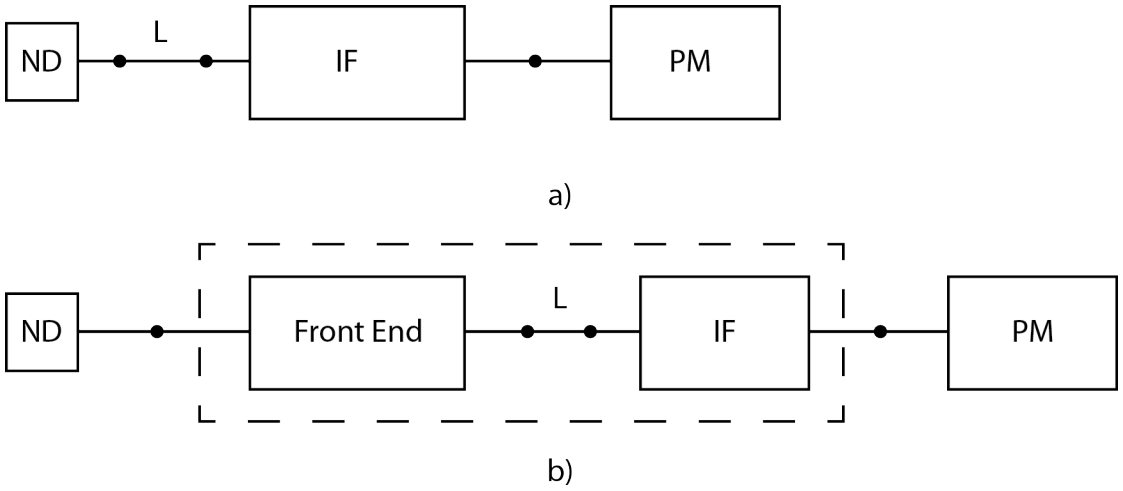

Figure E-2. Noise figure measurement configurations. ND represents the noise diode and PM represents the power meter.

APPENDIX F: CHARACTERIZATION RESULTS

This section contains test fixture characterization results for reference and magnetron front-ends. The results include gain, gain compression, and noise figure for the IF section, front-end, and system. In this section, gain and gain compression are measured with a continuous wave signal in the radar detection bandwidth. The 1-dB compression points are reported as input powers.

Tables F-1–F-3 show how IF gain, FE gain, and system gain are computed. Figures F-1–F-3 show how IF, FE, and system gain changed with input power. Finally, Tables F-4–F-6 show IF, system, and FE noise figures.

The IF 1 dB gain compression point is -25 dBm, both FE 1 dB gain compression points are -1dBm, and both system gain compression points are -32 dBm. Since the system GCPs are the same as the IF GCP minus the FE gain, we can conclude that the compression point for signals within the radar detection bandwidth is determined by the IF section.

Table F-1. IF gain.

Parameter	**Value**	**Calculation**
P_{SA} (dBm)	-15.0	-15.0
L_2 (dB)	0.2	0.2
P_{SG} (dBm)	-60.0	60.0
L_1 (dB)	0.2	0.2
G_{IF}(dB)		45.4

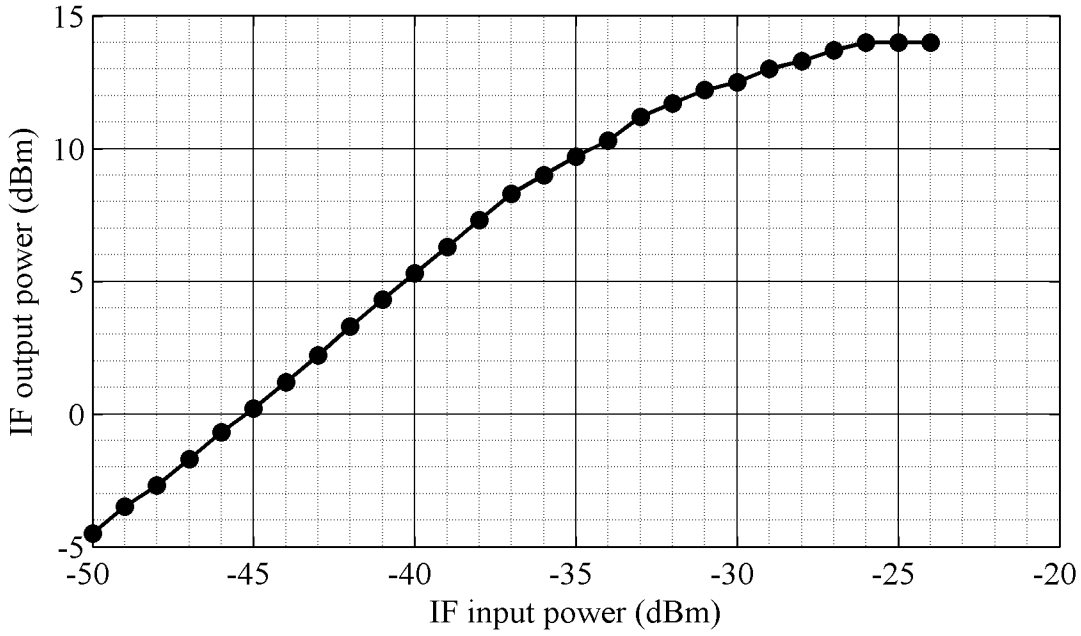

Figure F-1. IF gain compression.

Table F-2. FE gain.

Parameter	Reference Value	Reference Calculation	Magnetron Value	Magnetron Calculation
P_{SA} (dBm)	-45.67	-45.67	-45.0	-45.0
L_2 (dB)	0.2	0.2	0.2	0.2
P_{SG} (dBm)	-50.0	50.0	-50.0	50.0
L_1 (dB)	1.3	1.3	1.3	1.3
G_{FE} (dB)		5.83		6.5

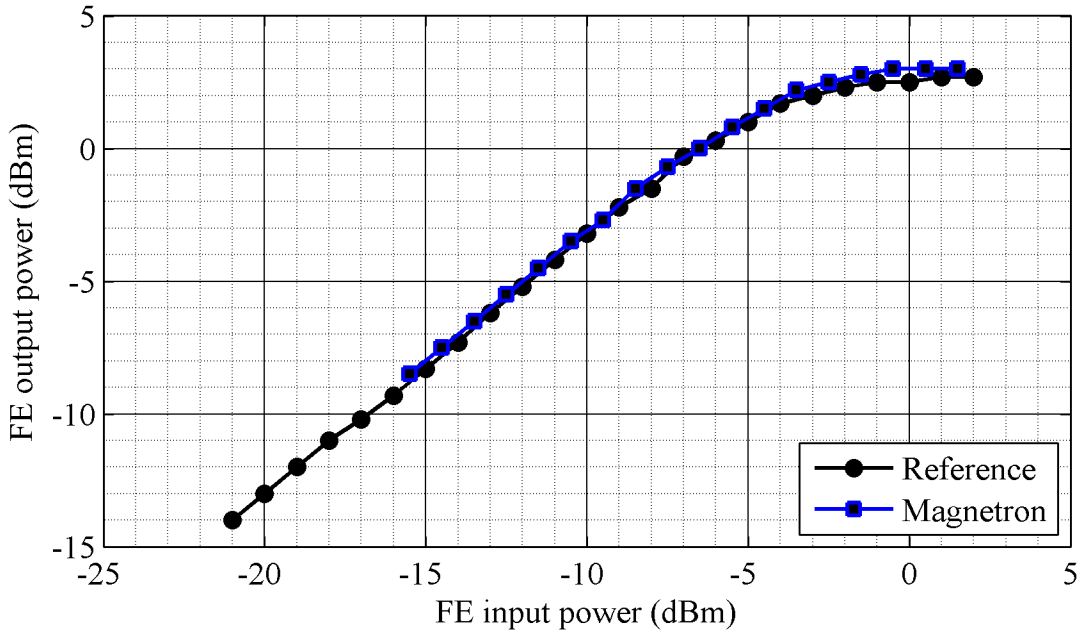

Figure F-2. FE gain compression.

Table F-3. System gain.

Parameter	Reference Value	Reference Calculation	Magnetron Value	Magnetron Calculation
G_{if} (dB)	45.4	45.4	45.4	45.4
G_{fe} (dB)	5.83	5.83	6.5	6.5
L_3 (dB)	0	0	0	0
G_{sys} (dB)		51.2		51.9

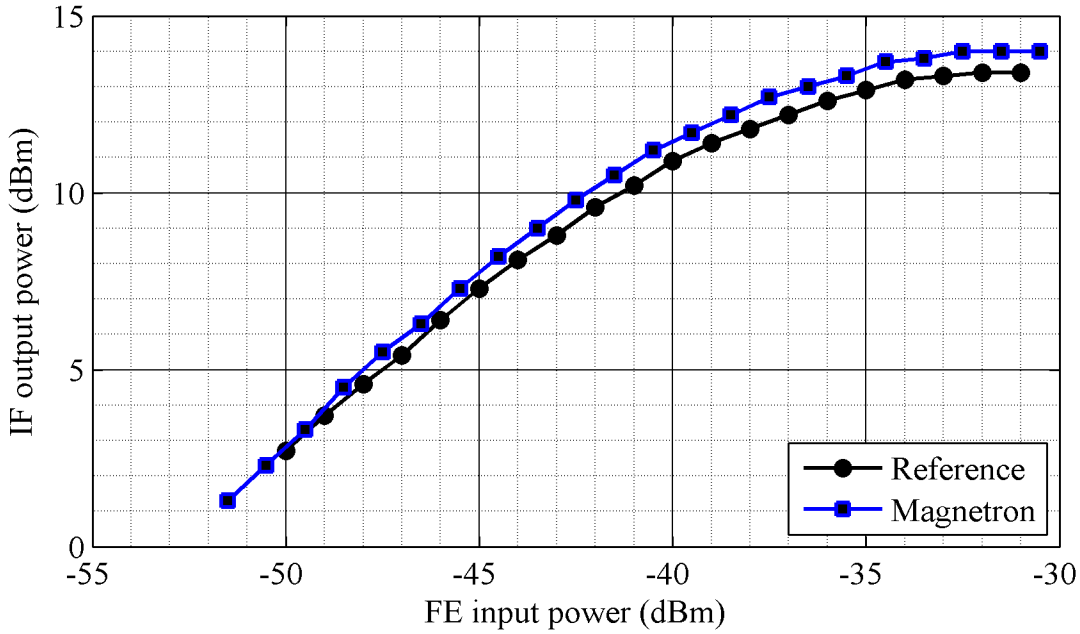

Figure F-3. System gain compression.

Table F-4. IF noise figure. Measured in 20 MHz IF bandwidth.

Parameter	**Value**
P_{on} (dBm)	-34.4
P_{on} (dBm)	-50.0
F_{if} (dB)	5.4

Table F-5. System noise figure. Measured in 20 MHz IF bandwidth.

Parameter	**Reference value**	**Magnetron value**
P_{on} (dBm)	-29.7	-28.7
P_{on} (dBm)	-44.3	-43.2
F_{sys} (dB)	5.85	5.95

Table F-6. Calculated FE noise figure.

Parameter	**Reference value**	**Magnetron value**
F_{sys} (dB)	5.85	5.95
F_{if} (dB)	5.4	5.4
G_{fe} (dB)	5.83	6.5
F_{fe} (dB)	5.04	5.3

APPENDIX G: VSG AND VSA SETUP

G.1 VSG Setup

The vector signal generator (VSG) provides the interfering signal. The interfering signal can originate from an internal generator within the VSG or a custom waveform file loaded into the VSG non-volatile waveform memory (NVWM) by the user. The internal generator could not provide the band limited Gaussian noise used to emulate the broadband radio service signal. Consequently we used a custom waveform file.

Automatic level control (ALC) is not possible with the widely varying Gaussian noise voltages. However, the average power can be monitored with the power detection loop. The only precaution necessary is to decrease power loop attenuation to compensate for the lower average power due to the Gaussian noise signal high peak to average power.

To manually set up the VSG:

1. Reset

2. Chose waveform

   If using a waveform:

   - If waveform is not loaded from NVWM:
     Mode>dual arb>select waveform>waveform segments> select waveform using dial or arrows >load segment from NVWM memory>return >highlight waveform using dial or arrows >select waveform

   - Else if waveform is loaded from NVWM
     Mode>Dual arb> select waveform >highlight waveform using dial or arrows >select waveform

   - If Gaussian noise or other signal with high peak to average ratio
     - Mode>Dual arb> arbsetup>mod atten set to manual and 6 dB.
     - Amplitude>ALC set to off, power search set to auto, power search reference set to modulated
     - Mode> Dual arb>Arb on

   If using modulation buttons:

   - Select modulation on front panel
   - Mod on button

If using a continuous wave:

- No need to do anything

3. Set frequency and amplitude

   - Frequency> set to RF center frequency
   - Amplitude> set to desired amplitude.
     Maximum amplitude is 20 dBm - 3 dB -peak/average in dB

4. Turn on RF

G.2 Creating Interfering Signal for the VSG

1. Create signal with MATLAB®
2. Save as .mat file
3. Run MATLAB program “Mat2Bin4VSG” to convert *.mat file to VSG binary *.bin file
4. Run MATLAB program “NormLargeBinFile4VSG” to convert *.bin file to normalized VSG binary file *.nor file
5. Use FTP to transfer *.nor file to VSG

G.3 VSA SETUP

To manually setup the VSA

1. Starting VSA

   - Unplug and plug in Firewire, power up VSA, start VSA software

2. Calibrate

   - Utilities>Single Cal

3. Modify setup

   - Measurement setup> Center frequency, Span, Resolution bandwidth, Data segment length
   - Input>Record>Record length
   - Input> Input range
   - File>Save>Save setup

4. Make recording

- Input>Data from hardware
- Input>Range
  Adjust to the highest level without overload when interference is present
- Control>Restart
- Control>Record
- File>Save>Save recording
- File naming convention: (Hardware configuration, VSG frequency, VSG power level).mat

G.3.1 VSA Setup Parameters

- Aliased cardinal span is

$$cardinal\ span = \frac{f_s}{2^n} \tag{G-1}$$

where f_s is the primary sampling rate and n is the cardinal span index.

- Usable or unaliased span is

$$span = \frac{cardinal\ span}{1.28} \tag{G-2}$$

- The time increment is

$$\Delta t = \frac{2^n}{f_s} \tag{G-3}$$

- The segment duration (mean time length) is

$$T_{seg} = N_{seg} \cdot \Delta t \tag{G-4}$$

where N_{seg} is the number of points in a segment

- The frequency spacing is

$$\Delta f = \frac{1}{T_{seg}} \tag{G-5}$$

- The total duration is

$$T = M \cdot T_{seg} \tag{G-6}$$

where M is the number of segments collected.

- The total number of points is

$$N = M \cdot N_{seg} \tag{G-7}$$

- For example, assuming a 95 MHz f_s
  - If n is 4, the cardinal span is 5.9375 MHz, the span is 4.638672 MHz, and Δt is 168.421 ns.
  - If N_{seg} is 1024, Δf is 5798.3 Hz, and T_{seg} is 172.463 μs
  - If M is 3000, T is 0.5173 seconds, and N is 3,072,000.

G.4 VSA Overload

The VSA can detect and report overloading, i.e. non-linear effects caused by strong signals, across its entire front-end bandwidth. Since the front-end bandwidth is greater than the measurement span, it is possible for the VSA to report overloading even though signals in the measurement span are within the instrument's dynamic range. Our policy is to monitor overload and not use data if it is detected.

G.5 SG and VSG Power Setting

This section describes how SG output power, P_{SG}, and VSG output power, P_{VSG}, are set relative to system noise power. Noise and signal power are also computed at the VSA input. In the calculations noise, N, signal, S, and interference, I, powers are those at the front-end (FE) input. Figure G-1 shows the front-end overload test fixture and parameters relevant for setting the powers.

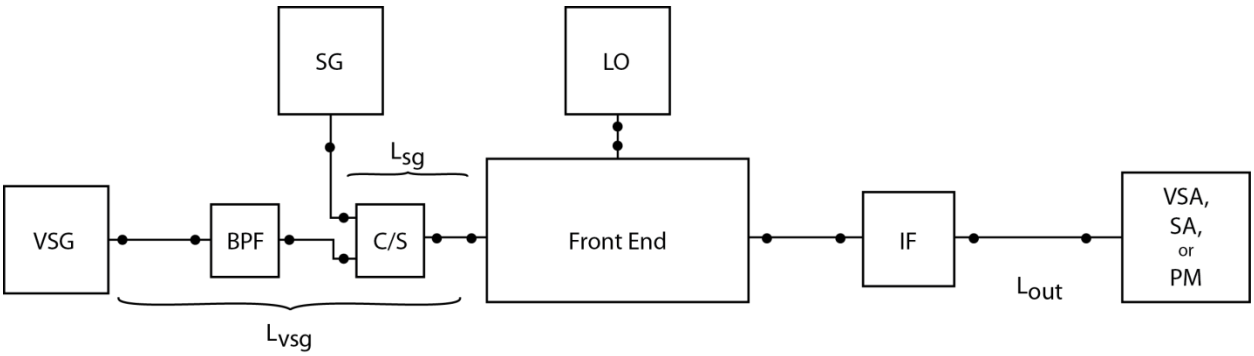

Figure G-1. Front-end overload test fixture. VSG represents the vector signal generator, BPF represents the band-pass filter, SG represents the signal generator, C/S represents the combiner/splitter, LO represents the local oscillator, VSA represents the vector signal analyzer, SA represents the spectrum analyzer, and PM represents the power meter. L_{SG}, $L_{VSG,}$ and L_{OUT} represent various losses.

1. Calculate noise power

$$N = kT + F_{sys} + B_{rad}\ (dBm) \quad \text{(G-8)}$$

where F_{sys} is the system noise factor referred to the FE input and B_{rad} is the radar noise equivalent bandwidth. In this case the radar noise equivalent bandwidth is equal to the VSA span.

2. Calculate P_{SG}

$$P_{SG} = SNR + N + K + L_{SG} + L_{misc}\ (dBm) \quad \text{(G-9)}$$

where SNR is the mean SNR over all target RCS fluctuations, K is the random Swerling radar cross section target RCS fluctuation factor, L_{SG}, is the loss from the SG to the FE, and L_{misc} are miscellaneous losses added to achieve baseline performance.

3. Calculate P_{VSG}

$$P_{VSG} = I + L_{VSG}\ (dBm) \quad \text{(G-10)}$$

where L_{VSG} is the loss from the VSG to FE.

4. The noise power at the instrument input is

$$P_{VSA} = N + G_{sys}\ (dBm) \quad \text{(G-11))}$$

where G_{sys} is the gain from the FE input to the instrument input. L_{out} was negligible.

5. The signal power at the instrument input is

$$S_{VSA} = SNR + N + G_{sys}\ (dBm) \quad \text{(G-12)}$$

L_{out} was also negligible.

The following tables show how N, P_{SG}, P_{VSG}, N_{VSA}, and S_{VSA} were computed for this test fixture. They are followed by calculations of signal and noise power measured by the VSA.

Table G-1. Noise power calculation.

Parameter	Units	Value		Note
		Reference	Magnetron	
kT	dBm/Hz	-174	-174	
F_{sys}	dB	5.85	5.95	
B_{rad}	dB-Hz	66.65	66.65	4.63 MHz VSA span
N	dBm	-101.5	-101.4	FE input

Table G-2. Swerling 0 no integration P_{SG} calculation.

Parameter	Units	Value		Note
		Reference	Magnetron	
SNR	dB	10.98	10.98	Swerling 0 no integrations (see Table G-6)
K	dB	0	0	Swerling RCS fluctuation factor
N	dBm	-101.5	-101.4	
L_{SG}	dB	4.5	4.5	Measured 12/18/12
L_{misc}	dB	0.5	-0.5	
P_{SG}	dBm	-85.52	-86.42	SG1 output

Table G-3. P_{VSG} calculation.

Parameter	Units	Value	Note
I	dBm	-20	
L_{VSG}	dB	5.8	Measured 12/18/12
P_{VSG}	dBm	-14.2	VSG output

Table G-4. Noise power measured by VSA in 4.63 MHz span calculation.

Parameter	Units	Value		Note
		Reference	Magnetron	
N	dBm	-101.5	-101.4	FE input
G_{sys}	dB	51.2	51.9	
N_{VSA}	dBm	-50.3	-49.5	VSA input

Table G-5. Swerling 0 no integration signal power measured by VSA calculation.

Parameter	Units	Value		Note
		Reference	Magnetron	
SNR	dB	10.98	10.98	Swerling 0 no integration (see Table G-6)
K	dB	0	0	Swerling RCS fluctuation factor
N	dBm	-101.5	-101.4	
S	dBm	-90.52	-90.42	
G_{sys}	dB	51.2	51.9	
S_{VSA}	dBm	-39.32	-38.52	VSA input

Table G-6. Mean SNR required without the interfering signal for various Swerling types and number of integrations.

Swerling type	Integrations	SNR (dB)
0	1	10.98
1	1	16.05

Swerling type	Integrations	SNR (dB)
0	6	4.83
1	6	10.03
0	14	2.31
1	14	7.58

APPENDIX H: INTERFERING SIGNAL GAIN COMPRESSION AND NOISE ENHANCEMENT MEASUREMENT SET UP

Interfering signal gain compression and noise enhancement were measured with the front-end overload test fixture. A block diagram of the test fixture is shown in Figure H-1.

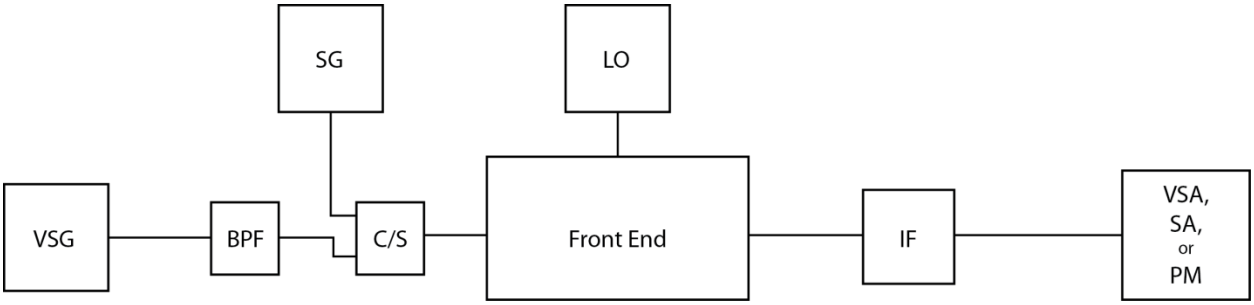

Figure H-1. Front-end overload test fixture block diagram. From left to right are the vector signal generator (VSG) which creates the BRS signal, band pass filter (BPF), power combiner/splitter (C/S), radar signal CW generator (SG), front-end, local oscillator (LO), intermediate frequency section (IF), and the test instruments including the vector signal analyzer (VSA), spectrum analyzer (SA), and the power meter (PM).

The radar signal is generated by the signal generator (SG) and the interfering signal is generated by the vector signal generator (VSG). To measure gain compression the radar signal amplitude is set well above the level that would be used for performance degradation measurements, but not so high that it would contribute significantly to front-end overload or cause the IF section to overload. With our test fixture we chose a -75 dBm radar signal amplitude at the front-end input. The radar signal amplitude was measured at the output of the IF section with a SA each time the interfering power was changed. Noise enhancement was measured in the same way in the absence of the radar signal.

Table H-1. Spectrum analyzer settings.

Parameter	**Setting**
Span	500 kHz
Resolution bandwidth	3 kHz
Video bandwidth	3 kHz
Sweep time	200 ms.
Attenuation	0 dB
Reference level	-10 dBm
Detector	Sample

FORM **NTIA-29**
(4-80)

U.S. DEPARTMENT OF COMMERCE
NAT'L. TELECOMMUNICATIONS AND INFORMATION ADMINISTRATION

BIBLIOGRAPHIC DATA SHEET

1. PUBLICATION NO.	2. Government Accession No.	3. Recipient's Accession No.
TR-15-515		

4. TITLE AND SUBTITLE	5. Publication Date
Effect of Broadband Radio Service Reallocation on 2900–3100 MHz Band Marine Radars: Front-end Overload	April 2015
	6. Performing Organization Code NTIA/ITS.T

7. AUTHOR(S)	9. Project/Task/Work Unit No.
Robert Achatz, Mark McFarland, Roger Dalke, Paul McKenna, Frank Sanders, Robert Johnk, Geoffrey Sanders	3105011-300
8. PERFORMING ORGANIZATION NAME AND ADDRESS Institute for Telecommunication Sciences National Telecommunications & Information Administration U.S. Department of Commerce 325 Broadway Boulder, CO 80305	10. Contract/Grant Number.

11. Sponsoring Organization Name and Address	12. Type of Report and Period Covered
U.S. Coast Guard Spectrum Management Telecommunications Policy Division U.S. Coast Guard CG-652, 2100 2nd St. SW Stop 7101 Washington, DC 20593-7101	

14. SUPPLEMENTARY NOTES

15. ABSTRACT (A 200-word or less factual summary of most significant information. If document includes a significant bibliography or literature survey, mention it here.)

Spectrum reallocations may place broadband radio services (BRS) near spectrum used by 2900–3100 MHz band marine radars. Signals from the BRS base stations can potentially cause the radar front-end to overload and cause interference. This report provides a method that can be used to estimate front-end filter attenuation required at various radar to base station separation distances. The attenuation is the difference between the interfering power at the radar low-noise front-end (LNFE) and the allowable interference power. The BRS signal was emulated with 10 MHz bandwidth Gaussian noise. The allowable interference power IPC is determined from probability of detection measurements with a custom test fixture. Two front-ends were tested. One was an off-the shelf magnetron radar front-end assembly consisting of a circulator, limiter, and low-noise front-end. The other, referred to as the reference front-end, was constructed of discrete components. The reference front-end was tested without the frequency selectivity of the circulator and limiter. Results showed that the allowable interference power is -11.5 and -9 dBm for the reference front-end and magnetron front-end assembly, respectively. Additional front-end filtering is not required for either front-end at distances as close as 400 meters. Distances less than 400 meters were not analyzed due to near-field effects. Gain compression and noise enhancement metrics, which are simpler to measure than performance degradation, were also evaluated to determine if they could reliably predict allowable interference power. Only the noise enhancement metric could reliably predict the performance degradation. This result is important since many front-end overload studies are based on the gain compression point metrics.

16. Key Words (Alphabetical order, separated by semicolons)
broadband radio service, front-end filter, front-end overload, gain compression, interference, interference protection criteria, marine radar, noise enhancement, radar, radio spectrum engineering, radio wave propagation

17. AVAILABILITY STATEMENT	18. Security Class. (This report)	20. Number of pages
☒ UNLIMITED.	Unclassified	95
☐ FOR OFFICIAL DISTRIBUTION.	19. Security Class. (This page) Unclassified	21. Price: N/A

NTIA FORMAL PUBLICATION SERIES

NTIA MONOGRAPH (MG)

A scholarly, professionally oriented publication dealing with state-of-the-art research or an authoritative treatment of a broad area. Expected to have long-lasting value.

NTIA SPECIAL PUBLICATION (SP)

Conference proceedings, bibliographies, selected speeches, course and instructional materials, directories, and major studies mandated by Congress.

NTIA REPORT (TR)

Important contributions to existing knowledge of less breadth than a monograph, such as results of completed projects and major activities.

JOINT NTIA/OTHER-AGENCY REPORT (JR)

This report receives both local NTIA and other agency review. Both agencies' logos and report series numbering appear on the cover.

NTIA SOFTWARE & DATA PRODUCTS (SD)

Software such as programs, test data, and sound/video files. This series can be used to transfer technology to U.S. industry.

NTIA HANDBOOK (HB)

Information pertaining to technical procedures, reference and data guides, and formal user's manuals that are expected to be pertinent for a long time.

NTIA TECHNICAL MEMORANDUM (TM)

Technical information typically of less breadth than an NTIA Report. The series includes data, preliminary project results, and information for a specific, limited audience.

For information about NTIA publications, contact the NTIA/ITS Technical Publications Office at 325 Broadway, Boulder, CO, 80305 Tel. (303) 497-3572 or e-mail info@its.bldrdoc.gov.